Contents lists available at ScienceDirect

Science of the Total Environment

journal homepage: www.elsevier.com

Contribution of isotopic research techniques to characterize high-mountain-Mediterranean karst aquifers: The Port del Comte (Eastern Pyrenees) aquifer

I. Herms[a], J. Jódar[b,*], A. Soler[c], I. Vadillo[d], L.J. Lambán[e], S. Martos-Rosillo[e], J.A. Núñez[a], G. Arnó[a], J. Jorge[f]

[a] Àrea de Recursos Geològics, Institut Cartogràfic i Geològic de Catalunya (ICGC), Barcelona, Spain
[b] Groundwater Hydrology Group, Dept. Civil Engineering and Environment, Technical University of Catalonia (UPC), Barcelona, Spain & Aquageo Proyectos S.L., Spain
[c] Grup de Mineralogia Aplicada i Geoquímica i Geomicrobiologia, Departament de Mineralogia, Petrologia i Geologia Aplicada, Facultat de Ciències de la Terra, Universitat de Barcelona (UB), Barcelona, Spain
[d] Centro de Hidrogeología, Universidad de Málaga (UMA), Málaga, Spain
[e] Instituto Geológico Minero de España (IGME), Spain
[f] Departament d'Enginyeria Minera, Industrial i TIC, Universitat Politècnica de Catalunya (UPC), Manresa, Spain

ARTICLE INFO

Article history:
Received 20 September 2018
Received in revised form 13 November 2018
Accepted 13 November 2018
Available online xxx

Editor: Damia Barcelo

Keywords:
Stable isotopes
Seasonal isotopic amplitude
Altitudinal line
Recharge
Mean transit time
Karst

ABSTRACT

Water resources in high mountain karst aquifers are usually characterized by high rainfall, recharge and discharge that lead to the sustainability of the downstream ecosystems. Nevertheless, these hydrological systems are vulnerable to the global change impact. The mean transit time (MTT) is a key parameter to describe the behavior of these hydrologic systems and also to assess their vulnerability. This work is focused on estimating MTT by using environmental tracers in the framework of high-mountain karst systems with a very thick unsaturated zone (USZ). To this end, it is adapted to alpine zones a methodology that combines a semi-distributed rainfall-runoff model to estimate recharge time series, and a lumped-parameter model to obtain MTT. The methodology has been applied to the Port del Comte Massif (PCM) hydrological system (Southeastern Pyrenees, NE Spain), a karst aquifer system with an overlying 1000 m thick USZ. Six catchment areas corresponding to most important springs of the system are considered. The obtained results show that hydrologically the behavior of the system can be described by an exponential flow model (EM), with MTT ranging between 1.9 and 2.9 years. These MTT values are shorter than those obtained by considering a constant recharge rate along time, which is the easiest and most applied aquifer recharge hypothesis when estimating MTT through lumped-parameter models.

1. Introduction

High mountain zones are known as "water towers" because they generate the main water resources feeding the most important rivers in the world (Viviroli et al., 2007). This phenomenon is especially important in the drought-prone Mediterranean area (Vicente-Serrano et al., 2014), where water availability is scarce and greatly dependent on runoff from headwater basins (De Jong et al., 2009). Moreover, water discharge from mountain areas is critical to ensure water supply in the lowland and coastal fringe (Viviroli and Weingartner, 2004; García-Ruiz et al., 2011), where human activity (agriculture, industry, tourism) concentrates.

Future scenarios for climate change in the whole Mediterranean region forecast an increase in temperature and a decrease in precipitation at the end of the 21st century (Giorgi and Lionello, 2008). These effects may well impact the Mediterranean high mountain zones (Nogués-Bravo et al., 2008; Lopez-Moreno et al., 2009; Ribalaygua et al., 2013), modifying the hydrological behavior of their headwater basins (Barnett et al., 2005; García-Ruiz et al., 2011, and references therein). Nevertheless, the first evidence of such changes has already been reported in the Pyrenees, the southernmost European range where glaciers can be found (Grunewald and Scheithauer, 2010). Pyrenean glaciers have undergone an intense retreat since the middle of the last century, causing most of them to face a certain close extinction (Chueca et al., 2007; René, 2013; Marti et al., 2015; López-Moreno et al., 2016). In addition, during this period, both mean annual precipitation and number of rainy days have shown a clear decreasing trend in this zone (Lopez-Moreno et al., 2010), along with a lesser snowfall and snow accumulation (López-Moreno, 2005). These effects directly impact the water storage capacity of the associated headwater systems (Seibert et al., 2015), as well as their associated hydrological response in terms of both river discharge flowrates and timing of maximum discharges (López-Moreno and García-Ruiz, 2004; Gremaud et al., 2009). These changes will directly impact the downstream zones by complicating the current water stress situation in the Mediterranean zone (Milano et al., 2013; Hernández-Mora et al., 2014; Molina and Melgarejo, 2016). Because of the hydrological outlook that is not so promising, it is essential to understand the functioning of the mountain hydrological systems of the Mediterranean area, especially those scenarios in which groundwater (GW) plays a major role in the headwater discharge, because mountain aquifers maintain base flows to rivers during the recurrent Mediterranean dry periods (Hoerling et al., 2012; Vicente-Serrano et al., 2014).

* Corresponding author.
Email address: jorge.jodar@hydromodelhost.com (J. Jódar)

https://doi.org/10.1016/j.scitotenv.2018.11.188
0048-9697/

Despite playing a strategic role, most high mountain hydrogeological systems are still insufficiently understood (Goldscheider, 2011). Conventional hydrogeological investigation techniques (Bakalowicz, 2005; Goldscheider and Drew, 2007) are often difficult to apply in alpine regions because of the difficult access and the harsh working conditions, along with the types of instruments needed for conducting research in high mountain zones (Lauber et al., 2014; Hood and Hayashi, 2010). However, a growing number of publications are focusing on the importance of groundwater in the functioning of high-mountain watershed rivers in different geological settings, including alluvial/rockfall/talus aquifers (Lauber and Goldscheider, 2014; Kurylyk and Hayashi, 2017), fractured aquifers (Jódar et al., 2017; Barberá et al., 2018a) and karst systems (Wetzel, 2004; Goldscheider, 2005; Gremaud et al., 2009; Mudarra et al., 2014; Allocca et al., 2015; Lambán et al., 2015; Chen, 2017; Barberá et al., 2018b; Kazakis et al., 2018). Determining the magnitude of groundwater recharge and aquifer Mean Transit Time (MTT) are key issues for understanding and managing alpine groundwater systems. Spring hydrograph analysis and environmental tracer methods allow for characterizing aquifer recharge and discharge processes, estimating recharge zone elevation and transit times, determining drainage structures, and assessing spring vulnerability, as well as calculating water resources in headwater aquifers (Wetzel, 2004; Rodgers et al., 2005; Einsiedl, 2005; Farlin and Maloszewski, 2013; Jódar et al., 2016b; Malard et al., 2016; Epting et al., 2018).

In high-altitude alpine karst aquifers, groundwater recharge processes highly depend on temporal and spatial distribution of precipitation and snowmelt (Lauber and Goldscheider, 2014). The estimation of MTT in karst systems is conditioned by the existence of variable flow conditions. These systems normally show triple-porosity and different connected parts: the karstic conduits that allows rapid flow, and the fissured-porous matrix that shows intermediate to slow flow. Artificial tracer test normally injected in preferential flow paths (i.e. the channels) doesn't consider the fissured-porous matrix of the aquifer, which can be important as far as the total karst water volumes (Małoszewski and Zuber, 2002). In this respect, the use of artificial tracers to characterize such hydrological systems is not enough since it doesn't allow characterizing all the components of the flow. Others important factors that govern the suitability of injection test for MTT estimations is the existence of a thick unsaturated zones (USZ): conducting tracer tests by injecting it at the surface of the thick USZ is likely a failing tracer test given the large uncertainties regarding the likelihood of hydraulic connection between the tracer injection point and the sampled system discharge point (Lauber and Goldscheider, 2014). Additionally, the adverse working conditions and the type of material of the instruments necessary to correctly perform the tracer test (Goldscheider et al., 2008) in high-mountain areas make it difficult to execute them.

As a result, the hydrogeological behavior of most of the mountain karst systems with an associated thick USZ remain uncharacterized, despite of being the exploration of these systems on the focus of speleogenetic research since the last decades (Ballesteros et al., 2015a, and references therein).

Lumped parameter models (LPMs) are useful to simulate the behavior of such complex mountain karst systems, even when they are poorly characterized. These models do not require a detailed hydrological knowledge of the physical system. Moreover, LPMs naturally integrate the USZ of the aquifer as a part of the whole hydrological system to be modeled (Turnadge and Smerdon, 2014). Additionally, the stable isotopes of water ($\delta^{18}O$ and $\delta^{2}H$) in rainfall have proved to be good environmental tracers for investigating the dynamics of such hydrological systems karst systems (Andreo et al., 2004). These tracers enter the system as recharge, migrate downgradient exploring the whole hydrological system, and leave the karst aquifer with spring discharge or by lateral mass transfer to other hydrogeologically connected aquifer units. In this line, this work is devoted to estimate MTT of a high-mountain karst aquifer with a thick unsaturated zone by using ^{8}O and ^{2}H as environmental tracers along with LPMs. To this end, it is considered the approach presented by Vitvar et al. (1999) to estimate MTT in a small Swiss pre-alpine aquifer. The original approach is adapted to high mountain zones by considering the existing vertical gradients of precipitation and air temperature along the slope of high mountains, but also the role played by the snow accumulation and ablation processes in the runoff generation. The resulting method combines in series two LPMs: (1) a semi-distributed rainfall-runoff HBV model (Bergström, 1976; Seibert, 2005) that simulates the observed hydrodynamical system response while taking into account the elevation dependences of the different hydrometeorological variables (i.e. Precipitation and temperature) and associated processes (e.g. snow accumulation and ablation), and (2) a FlowPC model (Małoszewski and Zuber, 1996) that estimates the mean transit time of the hydrological system while simulating the environmental tracer content evolution in the system discharge. This is done by numerically integrating a convolution integral (Małoszewski et al., 1983; Jódar et al., 2014). In our case, the FlowPC model uses as input data: a) the recharge time series of the aquifer obtained with the HBV model, and b) the time series isotope content ($\delta^{18}O$ and $\delta^{2}H$) in recharge, which is obtained through a spatiotemporal characterization of the isotope contained of precipitation.

The methodology is applied to the hydrological system of Port del Comte Massif (PCM; NE Spain), a karst aquifer with a 1000 m thick USZ. The hydrological system mainly discharges though the Cardener springs into the homonym river, which is the main tributary of the Llobregat River, the first water resources provider to the city of Barcelona (NE Spain). Despite the strategic role of Cardener springs the hydrologic behavior of the karst system remains unknown. This study contributes to a better hydrological characterization of PCM hydrological system. Moreover, the proposed methodology can be applied to characterize other high mountain karst aquifers with an overlying thick USZ that are common in many alpine zones elsewhere the globe.

2. Study area

The study area is located at the Port del Comte Massif (PCM), which is situated in the eastern part of the Pyrenees, NE Spain (Fig. 1). The elevation of the watershed ranges from approximately 900 m a.s.l., up to 2387 m a.s.l., at the 'Pedró dels Quatre Batlles' peak. With approximately 110 km^2, it contains one of the main mountain karst aquifers of the Catalan Pyrenees. The watershed of the massif divides the river basin of the Cardener River at the E and S and the river basin of the Segre River at the NW and SW. The massif constitutes an independent structural and hydrogeological unit.

2.1. Meteorological setting

From a climatic point of view, and according to the Köppen-Geiger classification (Peel et al., 2007), the study zone has a cold climate without dry season and temperate summer (defined as 'Dfb' type; accordingly to Agencia Estatal de Meteorología de España (AEMET) and Instituto de Meteorologia – Portugal (IMA), 2011). At the meteorological station MS-01 (Fig. 1), which is located at 2315 m a.s.l., the average values of precipitation (P), temperature (T) and potential evapotranspiration (ETP) calculated with the Hargreaves and Samani (1982) equation are 1055 mm/yr, 3,24 °C and 525 mm/yr, respectively. These three variables show a seasonal variation (Fig. 2) and an elevation dependence. The measured vertical gradients (lapse rate) of precipitation ($\nabla_z P$), atmospheric temperature

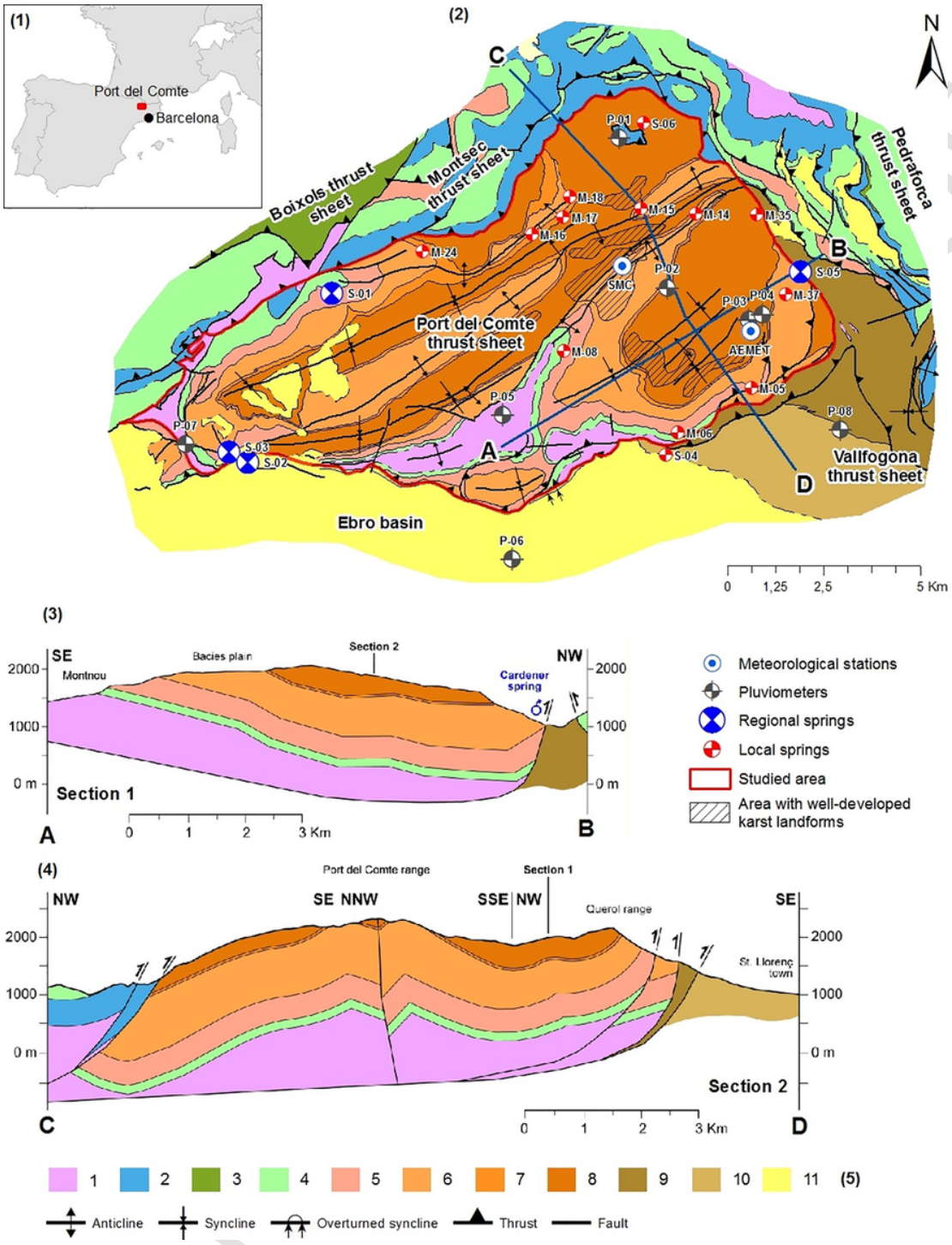

Fig. 1. (1) Location map of the study zone. (2) Geological map (geological map modified from ICGC, 2007). (3) Geological cross-section A–B. (4) Geological cross-section C–D. (5) Geological legend: [1] Triassic – shales, limestones, dolomites and evaporates; [2] Jurassic – marls, bioclastic limestones and dolomites; [3] Lower Cretaceous – mudstones, ammonite limestones and marl; [4] Upper Cretaceous – limestones, marls, calcarenites and terrigenous deposit; [5] Garumnian – red shales and limestones; [6] Lower Eocene – fissured and karstified alveoline limestones and dolomites; [7] Lower Eocene – marls, sandstones and limestone; [8] Lower Eocene – fissured and karstified micritic and bioclastic limestones; [9] Middle Eocene – sandstones, marls, conglomerates, limestones and evaporates; [10] Upper Eocene – continental alluvial systems: conglomerates and sandstones; [11] Oligocene – continental alluvial systems: conglomerates, breccias and sandstones.

(∇_zT) and potential evapotranspiration (∇_zETP) are 8,9 mm/yr/100 m, −0,74 °C/100 m and −32,3 mm/yr/100 m, respectively. The snow cap is present in the upper zones of the basin in winter and spring, maintained annually for 3 to 4 months since 1800 m a.s.l., meaning that precipitation is partly produced as snow.

Despite the high average rainfall above 1000 mm/year, in most of the study area the surface runoff is almost nonexistent, and it is not observed until reaching lower altitudes.

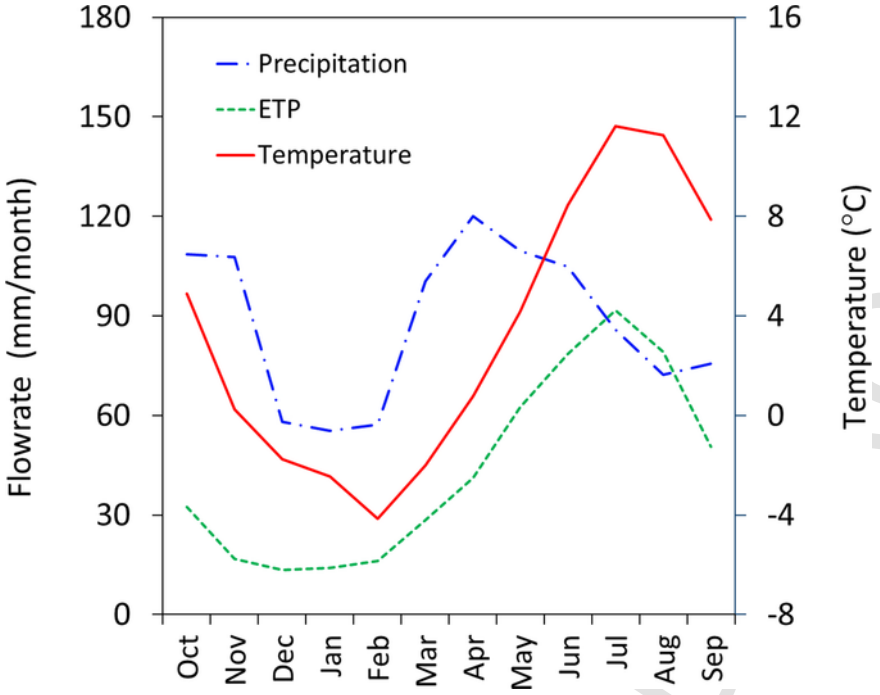

Fig. 2. Seasonal variation of precipitation, potential evapotranspiration and temperature measured at the meteorological station MS-01 (see Table 1) located at 2315 m a.s.l. for the period Sep 2005–Apr 2016.

2.2. General settings of the study zone

From a geological perspective, the massif belongs to the PCM thrust sheet that presents complex structural relationships in its contours (Fig. 1). On the E, the PCM mantle borders on the mantle of Cadí, coinciding with the point of origin for the Cardener River (spring S-05; Fig. 1). To the NE and NW, the PCM is limited by the tectonic plates of the mantles of Sierras Marginales, Montsec and Boixols. To the S, the PCM mantle overlaps with the conglomeratic materials of the Ebro Basin, the southern foreland basin of the Pyrenees. The internal structure of the PCM mantle is formed by a set of folds and thrusts detached above the Triassic. These folds have a constant direction NE–SW parallel to the NW limit of the mantle (Vergés, 1999). The stratigraphic series contains materials from the Triassic, Jurassic, Cretaceous and Paleogene with a total of approximately 1000 m thickness. The main karst aquifer inside PCM massif is in the Paleocene–Eocene carbonate rocks. The geologic structure and stratigraphy of the PCM thrust strongly influence the location of the existing karst springs, their groundwater geochemistry and their hydrologic behavior. The lower Upper Cretaceous/Paleocene (Garumnian facies) substrate materials underlying the Paleocene aquifer are composed of sandstone, siltstone and shale. These materials constitute an impervious layer for the overlaying aquifer system.

From the geomorphological point of view, the PCM has a characteristic triangular geometry. The PCM has a smooth rounded landscape with a plain in the highest part without vegetation cover and with almost no soil, which corresponds to approximately 10% of the total area. The rest of the massif is covered by mountain meadows (29%) and forest (61%) with scarce soil depth up to medium developed soil cover. Different karstic forms progressively appear from 1950 m a.s.l. upwards, being well developed at 2050 m a.s.l., with sinkholes, dry caves, dolines and karren fields, generating a heterogeneous karstified hydrogeological system.

The hydrogeological conceptual model of the PCM aquifer system considers that recharge is produced by infiltration of precipitation as rainfall and snowmelt. The magnitude and distribution of infiltration is conditioned by the development of the karst landforms. The infiltration is produced (1) in a concentrated way through the local karstic elements such as dolines and (2) in a diffuse way by rain and snowmelt along the whole PCM area. The epikarst unsaturated zone (NSZ) presents a thickness close to 1000 m in the highest zones of the PCM. The infiltrated water flows vertically through the NSZ towards the saturated zone.

The hydrogeological system naturally discharges through the large number of existing springs. Approximately 100 springs have been found in the PCM showing large discrepancies in their mean discharge flow rate, ranging from values ≪1 L/s up to values >100 L/s. Most of these springs discharge a local subhorizontal interflow characteristic of a small entity (i.e., Local springs, Table 1). However, in terms of groundwater discharge, there are six important springs in the PCM (i.e., Regional springs, Table 1). These springs have been monitored regularly for this research, showing that all of them have a highly variable discharge flow rate (Fig. 3). Four of these regional springs (S-01, S-02, S-03 and S-05) are the principals discharging points of the whole hydrogeological system. The four springs are located at elevations between 944 and 1098 m a.s.l. (see Table 1). Through these main springs, the hydrogeological system discharges at two principal watersheds: the Cardener River watershed to the east and the Segre River watershed to the northwest. Groundwater flow direction is conditioned by the geological structure of PCM. Nevertheless, the exact position of the regional groundwater table is poorly known.

3. Materials and methods

3.1. Field work

To collect precipitation samples, a network of 8 cumulative precipitation gauges (pluviometers) of the type CoCoRaHS RG202 Official-4 was installed at elevations between 896 and 1935 m a.s.l. (P-01

Table 1
Meteorological stations, pluviometers and springs in the study zone sampled during the period July 2013–October 2015.

Code	Type	Name	Elevation (m a.s.l.)	Num. water samples (–)	Discharge rate (L/s)
MS-01	Met. Station	SMC-Z8	2315	–	–
MS-02	Met. Station	AEMET-0127O	1800	–	–
P-01	Pluviometer	Refugi de l'Arp	1936	7	–
P-02	Pluviometer	Bassa Clot de la Vall	1946	8	–
P-03	Pluviometer	Refugi Bages	1768	8	–
P-04	Pluviometer	Casa X&A	1657	8	–
P-05	Pluviometer	Casa Ramonet	1450	8	–
P-06	Pluviometer	Casa Cavallera	1216	7	–
P-07	Pluviometer	Camp. La Comella	1062	8	–
P-08	Pluviometer	Camp. Morunys	896	9	–
S-01	Regional Spring	Font Aiguaneix	1098	25	8–73
S-02	Regional Spring	Font Sant Quintí	944	25	70–575
S-03	Regional Spring	Font Can Sala	1062	25	0,25–148
S-04	Local Spring	Font Coll de Jou	1464	25	0,07–0,59
S-05	Regional Spring	Fonts del Cardener	1032	25	57–904
S-06	Local Spring	Font carretera Refugi Arp	1858	25	0,04–7
M-05	Local Spring	Font del Ginebró	1730	4	<0,001
M-06	Local Spring	Font de la Garganta	1657	4	0,02–0,49
M-08	Local Spring	Font Orris 02	1871	4	0,1–0,7
M-14	Local Spring	Font Estivella	2053	4	0,07–5
M-15	Local Spring	Font Arderic	2158	3	0,03–2,8
M-16	Local Spring	Font del Casalí	2077	1	<0,001
M-17	Local Spring	Font del Diumenge	1989	2	0,004–0,026
M-18	Local Spring	Font barraca Sangonella	1940	1	0,001–0,01
M-24	Local Spring	Font dels Acens	1550	4	0,06–0,23
M-35	Local Spring	Font Ca l'Arreplagant	1330	4	<0,001–0,02
M-37	Local Spring	Font La Part (esllav.)	1315	4	0,5–1

a P-08; Fig. 1). The pluviometers consist of a polycarbonate cylindrical deposit with a diameter of 10,8 cm. The pluviometers include a top funnel that captures and guides precipitation into the storing deposit, where according to the technical procedure for the stations of the Global Network of Isotopes in Precipitation (GNIP) of the International Atomic Energy Agency (IAEA), a 0,5 cm paraffin oil floating layer is added to avoid evaporation. The pluviometers were sampled seasonally (except the first winter with two campaigns), a total of 9 campaigns from Dec. 2013 to Dec. 2015. Additionally, one snow sampling survey was conducted in December 2003. The snow samples were obtained by drilling through the entire snow depth (Lambán et al., 2015) and were taken at different locations with elevations ranging from 1935 to 2150 m a.s.l.

Groundwater samples were collected under different hydrodynamic conditions between Oct. 2013 and Dec. 2015. In this period, the springs S-01 to S-06 were sampled approximately monthly, for a total of 25 sampling campaigns. Groundwater samples were taken before the snow arrival in autumn (Oct. 2013 and Oct. 2014), and after the snow-melting season (Apr. 2014 and Apr. 2015). In these springs, groundwater discharge was measured once every two weeks from Jul. 2013 to Oct. 2015 (Fig. 3). In springs S-01, S-02, S-03 and S-05 the discharge flow rate was measured by conducting slug-injection salt dilution tests (Cervi et al., 2014), whereas the volumetric method was used for the precision discharge measurement in springs S-04 and S-06. The M-## springs (Table 1) showed a tiny and intermittent discharge. Therefore, groundwater samples were only taken with uneven frequency when it was possible.

The isotopic composition (δ^2H and $\delta^{18}O$) of all low salinity water samples was determined in the Center of Hydrogeology of the University of Málaga (CEHIUMA), where a Picarro® "L2130-I" isotopic water analyzer was used. The analytical uncertainties for $\delta^{18}O$ and δ^2H are ±0.2‰ and ± 1.0‰, respectively. According to Coplen (2011) several international and laboratory standards have been interspersed for normalization of analyses. The standards used (WICO-13, WICO-14, WICO-15) were calibrated in an interlaboratory comparison (Wassenaar et al., 2012). All results are given relative to the V-SMOW standard.

3.2. Approach for spring catchment delineation

A critical aspect to understand the behavior of karst hydrogeological flow systems is the delineation of the spring capture zones (i.e., recharge areas) and their boundaries (Goldscheider and Drew, 2007). Ideally, the delineation should be based on the proven information of connection between recharge areas and the discharge points. In high mountain zones, this connection may be confirmed by conducting tracer tests (Goldscheider et al., 2008; Mudarra et al., 2014; Barberá et al., 2018b). When this information is not available, the spring capture zone can be indirectly inferred by considering inputs from other classical information sources such as geophysics, structural geology and geomorphology data interpretation. However, 3D conceptual modeling techniques are currently being used to delineate the spring capture zones: Malard et al. (2015) analyze spring discharge hydrographs based on geological three-dimensional (3D) conceptual modeling (Butscher and Huggenberger, 2007, 2008; Martos-Rosillo et al., 2014; Ruiz-Constán et al., 2015; Malard et al., 2015; Ballesteros et al., 2015b; Epting et al., 2018).

In this work, a combined 3D conceptual methodology has been used to delineate the catchment areas associated with each spring. The delineating criteria are based on the information provided by three complementary methods: (1) the interpretation of the geological structure and the subsurface catchments relative to each spring location. To this end, a 3D geological model has been developed in the 3D-Move software platform (Midland Valley Exploration Ltd.); (2) the analysis of the disposition and location of the karst landforms over the area, and (3) the analysis through GIS spatial analysis tools of the ground surface structure, including type of soils (CREAF, 2009) and vegetation (Appendix A) at the spring recharge elevation zones. In the case of the regional springs S-01, S-02, S-03 and S-05, the three listed methods have been applied to delineate their catchment zone, whereas in the case of the perched springs S-04 and S-06, only the previous methods (2) and (3) could be applied. Fig. A1 (Appendix A) shows the catchment zones (i.e., aquifer units) obtained for the selected springs.

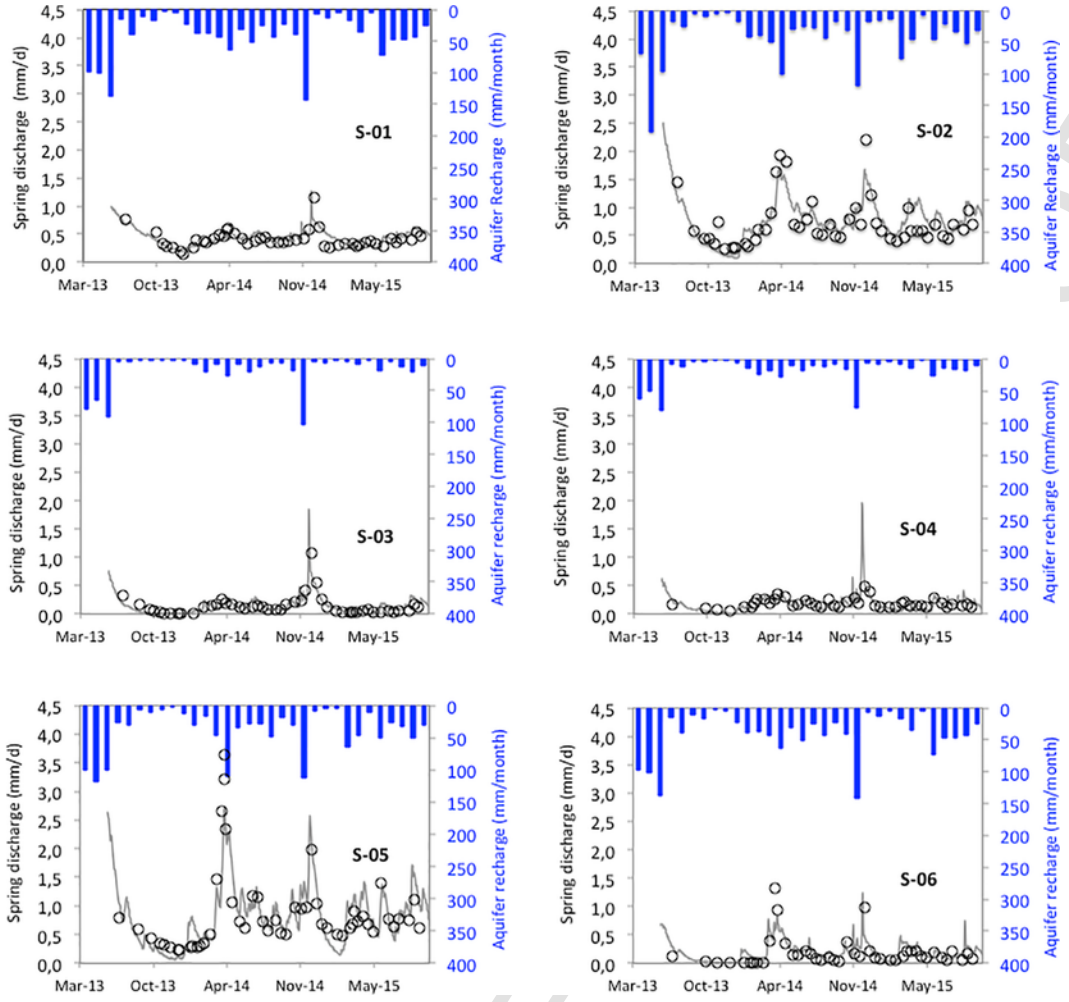

Fig. 3. Measured spring discharge (circles) in the six monitored springs (S-01 to S-06, Table 1) of the PCM hydrogeological system. Gray lines indicate the spring discharge numerically simulated with the HBV model (Seibert and Vis, 2012). For each spring, blue columns indicate the recharge values time series used as input data to the corresponding HBV model. (For interpretation of the references to colour in this figure legend, the reader is referred to the web version of this article.)

The delineated catchment zones associated with the regional springs divide PCM into two main blocks: (1) a southwestern block that includes only the catchment zone associated with S-05. This catchment zone is characterized by a syncline dipping NW structure (Fig. 1). From a functional point of view, this zone is hydrodynamically independent of the rest of PCM given the existence of an anticline and a main NE-SW fault that prevents lateral flows. (2) The northeastern block formed by the catchment zone associated with springs S-01, S-02 and S-03. The geological structure of this block regulates the regional groundwater flows, so as the Alinyà anticline controls the discharge of spring S-01, and the main syncline-anticline system dips SW along with the minor faults and synclines dipping south conditions the discharge of springs S-02 and S-03. Table A1 (Appendix A) provides the geographical details of the delineated groundwater catchment zones.

3.3. Characterizing the seasonal variation of environmental tracers

The evolution of some environmental variables is linked to the atmospheric temperature variation. As a result, these variables often show a similar seasonal pattern that can be characterized with a general sinusoidal function $\delta(t)$ (Jódar et al., 2014). This function consists of two additive terms, a sine-wave function [Eq. (1)] plus a temporal linear trend for the mean [Eq. (2)].

$$\delta(t) = A\sin\left(\omega\left(t - t_0\right) + \varphi\right) + \overline{\delta} \tag{1}$$

$$\overline{\delta} = \alpha\left(t - t_0\right) + \overline{\delta_0} \tag{2}$$

where A is the amplitude of the sinusoidal function, ω is the angular frequency, φ is the angular initial at time t_0, α is the slope of the linear trend, and $\overline{\delta_0}$ is the linear trend value at time t_0. The parameters A, α and $\overline{\delta_0}$ can be estimated by using the solution of any of the commonly available spreadsheet software's or manually. In this work, the root-mean-squared error (RMSE) is used as the selection criterion for the best fit to the measured isotope content time series.

In the case time series with a short amount of data (e.g., associated with the M-## springs in Table 1), it is not possible to obtain reliable estimates for, α, A, and $\overline{\delta_0}$ by using the method proposed above. In this case, no linear trend in the mean value is assumed ($\alpha = 0$), and $\overline{\delta_0}$ and A are estimated as:

$$\overline{\delta_0} = \frac{1}{N}\sum_{i=1}^{N}\delta_i \quad (3)$$

$$A = \max\left(\mathrm{Abs}\left(\overline{\delta_0} - \delta_i\right)\right); \forall i = 1 \div N \quad (4)$$

where N is the number of the isotopic content value of the time series.

Hydrogeological systems transfer the isotopic input signal of recharge. The tracer input seasonal signal is buffered and delayed as it propagates through the aquifer towards the discharging point (Fig. 4). This tracer transport process through the hydrological system can be described by the convolution integral that relates the tracer input content in recharge δ_{in} to the tracer input content in the spring discharge δ_{out} as shown below.

$$\delta_{out}(t) = \int_{-\infty}^{t} \delta_{in}(t)\, g\left(t - t'\right) dt' \quad (5)$$

where t is the time of tracer entry as recharge, t' is the integration variable and $g(t')$ is a weighting function describing the Transit Time Distribution (TTD) exit of tracer content that entered the aquifer at different times in the past. The differences between the input and the output tracer signals are related to the aquifer system MTT (τ) which is the first moment of the system TTD and is given by

$$\tau = \int_0^{\infty} t g(t)\, dt \quad (6)$$

where V is the volume of mobile water in the system (Małoszewski et al., 1983), and Q is the volumetric flow rate through the system. In the case of natural gradient hydrogeological systems, MTT corresponds to the mean amount of time for groundwater to travel from the recharge zone to the discharging spring. In this situation, MTT is related to the spring discharge flow rate Q, and the aquifer storage Vas follows (Custodio and Llamas, 1976):

$$\tau = \frac{V}{Q} \quad (7)$$

Additionally, in natural gradient hydrogeological systems with a seasonal varying input tracer function, MTT can be estimated as (Małoszewski et al., 1983):

$$\tau = \frac{1}{\omega}\sqrt{\left(\frac{A_{\delta_{in}}}{A_{\delta_{out}}}\right)^2 - 1} \quad (8)$$

where $A_{\delta_{in}}$ and $A_{\delta_{out}}$ are the amplitudes of the seasonal variation of the isotopic content in the aquifer recharge and the spring discharge, respectively. As can be shown, the above equation compares $A_{\delta_{in}}$ with respect to $A_{\delta_{out}}$,so the larger the amplitude dampening is, the longer the transit time.

3.4. Numerical approach for simulating the aquifer behavior

To reproduce the observed spring discharge flow rates and the associated isotopic content, a two-step methodology has been used:

(1) Simulation of the hydrodynamic behavior of the hydrogeological system. To this end, the freely available version of the semi-distributed conceptual precipitation–runoff model HBV-Light (Seibert and Vis, 2012) is used. HBV is a conceptual rainfall-runoff model for catchment hydrology modeling that solves a general water balance equation. HBV has been used in different alpine mountain hydrologic research studies (Braun and Renner, 1992; Hottelet et al., 1993; Uhlenbrook et al., 1999; Merz and Blöschl, 2004; Konz and Seibert, 2010; Staudinger et al., 2017; Epting et al., 2018; Jódar et al., 2018). This model has become a standard tool for simulating high mountain snow-dominated hydrological systems. This code requires as input data some hydroclimatic catchment information such as the relative weight with respect to the total area of the different altitude and associated vegetation zones in the catchment, the vertical lapse rates ∇_zP and ∇_zT, as well as the time series of daily P, T, and ETP. The hydrological catchment can be separated into numerous elevation zones, depending on the elevation gap between the lowest and the highest points of the catchment. In this work, every zone has been divided into three elevation zones (Table A1 in Appendix A). Additionally, every elevation zone can be divided into different vegetation zones. Based on the Land Cover Map of Catalonia (CREAF, 2009), three vegetation zones are considered: (1) open areas corresponding to zones of both poor or no soils where karst landforms are very well-developed (karren fields, sinkholes, dolines, etc.), (2) areas with mountain meadows and soil moderately developed, and (3) alpine forest zones with moderate to well-developed soils. A two stacked linear reservoir is used to simulate the hydrological system dynamics. The upper reservoir is used to generate surface and subsurface runoff whereas the lower reservoir generates groundwater runoff. The model considers vegetation zones parameters and catchment zone parametrer (Tables C1 and C2 of Appendix C, respectively). They are can be automatically calibrated by minimizing an efficiency objective function (R_{eff}; Table C3, Appendix C), which is already implemented in

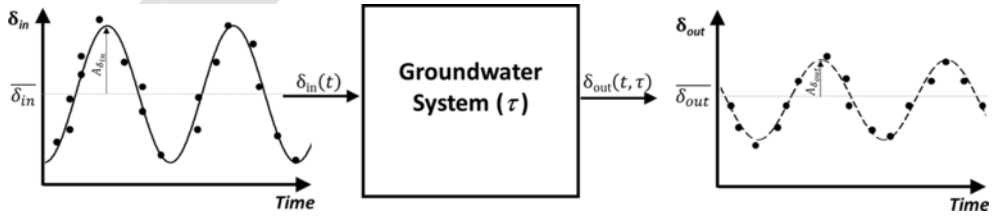

Fig. 4. Schematic representation of the groundwater system response $\delta_{out}(t, \tau)$ to a hypothetical input tracer function $\delta_{in}(t)$ (modified from Jódar et al., 2016b), where τ means MTT.

HBV. The model output includes the daily time series of aquifer recharge Q_R, which is used in the following step.

(2) Simulation of the transient isotopic content variation in the groundwater discharge. The temporal variation of the isotopic content in the spring discharge is simulated with FlowPC (Małoszewski and Zuber, 1996, 2002), a lumped parameter model typically used to estimate groundwater MTTs with the aid of observed environmental tracer data (Viville et al., 2006; Einsiedl et al., 2009; Katsuyama et al., 2010; Lauber and Goldscheider, 2014; Sánchez-Murillo et al., 2015; Mądrala et al., 2017). The program solves the convolution integral [Eq. (5)] and transforms the isotopic input tracer signal $\delta_{in}(t)$ entering the hydrogeological system as recharge into the isotopic output tracer signal $\delta_{out}(t)$ leaving the system through the spring discharge. To this end, FlowPC includes among others two parametric TTDs which are especially well suited for simulating karst aquifer systems: (A) The exponential model (EM), also known as a "good mixing model", is typically applied in systems where the groundwater flow lines tend to converge towards the water sampling points (Zuber, 1986; Amin and Campana, 1996). (B) The Exponential-Piston model (EPM) or "real system model", which combines two parts in line, an unconfined upstream part where recharge enters the system and an exponential distribution of transit times is assumed, and a confined downstream part where the flow scheme is approximated like the piston flow model (Zuber, 1986). The weighting function for EPM is described by the following equation.

$$g(t) = \begin{cases} 0 & t < \tau\left(1 - \frac{1}{\eta}\right) \equiv t_\tau \\ \frac{1}{\tau}\eta e^{-\frac{\eta}{\tau}+\eta-1} & t \geq t_\tau \end{cases} \quad (9)$$

where η is the ratio of total volume of the hydrogeological system to the volume of the system in which the exponential TDD exists, and τ is MTT. [Eq. (9)] also describes the EM weighting functions when $\eta = 1$, which is the lowest bound of this parameter. The model parameters (η and τ) are calibrated by minimizing the RMSE function.

FlowPC requires the time series of (1) monthly aquifer recharge $\widehat{Q_R}$ (hereinafter, a circumflex accent over a flow or an isotopic content variable indicates that the variable is cumulated monthly or averaged, respectively), which is obtained from the HBV model outputs for each simulation, and (2) the corresponding monthly averaged isotopic content of the recharge $\widehat{\delta_R}$. Given the karstic nature of the hydrogeological system, we assume that the isotopic content of local recharge and its seasonal characteristics (i.e., $\overline{\delta}_{in}, A_{\delta_{in}}$) are the same as the isotopic content and seasonal characteristics of local precipitation ($\overline{\delta}_P, A_{\delta_P}$). Since $\overline{\delta}_P$ and A_{δ_P} are known, then $\delta_P(t)$ is analytically obtained through [Eq. (1)]. As $\delta_P(t)$ is a daily time function, it is necessary to transform it into $\widehat{\delta_P}$. For the j^{th} month, $\widehat{\delta_{Pj}}$ is obtained by weighting the daily values of recharge isotopic content $\delta_{P_{ij}}$ by the corresponding daily recharge rate $Q_{P_{ij}}$ as

$$\widehat{\delta_{Rj}} \sim \widehat{\delta_{Pj}} = \frac{\sum_{i=1}^{N} \delta_{P_{ij}} Q_{R_{ij}}}{\sum_{i=1}^{N} Q_{R_{ij}}} \quad (10)$$

where N is the number of days of the j^{th} month. The Appendix D includes all the technical details corresponding to the different FlowPC models used in this work.

3.5. Statistical analysis of the relationship between the infiltration coefficient and recharge

To analyze the factors that controls the mean calculated infiltration coefficient (ξ) in the PCM, a linear regression model has been built, expressing the dependent variable ξ as a linear function of N explanatory variables Ψ_i as

$$\xi = \lambda_0 + \sum_{i=1}^{N} \lambda_i \Psi_i \quad (11)$$

where λ_0 is the intercept (constant) term, and λ_i ($i \geq 1 \div N$) are the regression coefficients associated with the predictors Ψ_i. In this study, the predictor variables of the linear regression model of the [Eq. (11)] are the elevation of the spring recharge zone Z_R (Table 3), the mean precipitation at the spring recharge zone P_{ZR} (Table 6), and the percentages of open areas, mountain meadows and forest in the spring catchment zones (VZ_1, VZ_2 and VZ_3, respectively; Table A1 in Appendix A). The coefficient of determination of the regression is one, so the model reproduces the whole variance of ξ. Table 7 shows the intercept value λ_0, the regression coefficients λ_i, and their corresponding standardized value β_i ($i \geq 1 \div N$). The standardized value β_i measures the expected change in ξ, in standard deviation units, for a one standard deviation change in Ψ_i, provided that other explanatory variables in the model (Ψ_j, $\forall i \neq j$) are fixed (Nimon and Oswald, 2013). The larger the absolute value of β_i, the more important the corresponding predictor Ψ_j is.

4. Results and discussion

4.1. Results from observed data

The isotopic content of the precipitation corresponding to the water samples taken is shown in Fig. 5A. The mean isotopic content of precipitation is lighter in winter and autumn than that in spring and summer, as one would expect given the dependence between the isotopic content in rainfall and temperature (Mook and De Vries, 2000). The obtained values are aligned between the Global Meteoric Water Line (GMWL) and the West Mediterranean Meteoric Water Line (WMMWL) (Fig. 5A). The local water meteoric water line (LMWL) that is obtained by linear regression (N=76; R^2=0,97) is defined as $\delta^2H = 8{,}05 \cdot \delta^{18}O + 12{,}74$. From a seasonal point of view, the isotopic content of precipitation in autumn and winter presents a larger variability than the isotopic content of precipitation in spring and summer, as shown in Fig. 5B by the error bars indicating the standard deviation associated with every seasonal value. The isotopic content in groundwater changes seasonally much less, than the isotopic content in precipitation (Fig. 5B), pointing out the existence of a good mixing flow process in the discharging points of the aquifer.

The geographical location of the study zone postulates the Mediterranean as the most important source of precipitation. This assumption is supported by the overall mean deuterium excess ($dex = \delta^2H - 8 \cdot \delta^{18}O$) value of 12,03 ± 3,37‰ obtained for all the precipitation samples analyzed (Celle-Jeanton et al., 2001; Jiménez-Martínez and Custodio, 2008). Nevertheless, the Atlantic fingerprint in rainfall can be observed in the above *dex* value through its variation interval, which provides a minimum *dex* value of 8,66‰ (Froehlich et al., 2001; Araguás-Araguás and Díaz-Teijeiro, 2005).

The isotopic composition of precipitation and spring discharge show a seasonal variation, which is not reflected in the deuterium excess. A seasonal variation in *dex* would indicate the existence of different moisture sources generating rainfall in the study zone by fol-

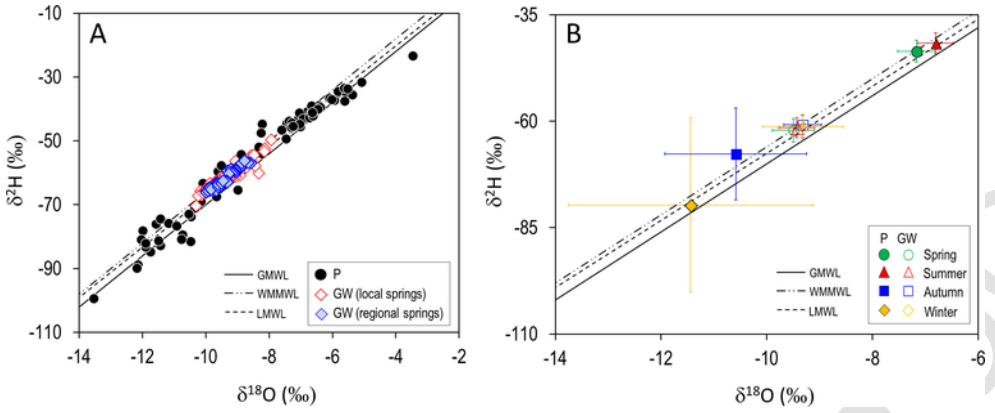

Fig. 5. (A) Values of $\delta^{18}O$ and $\delta^{2}H$ in precipitation (P; solid circles) and groundwater (GW) from local springs (empty red diamonds) and from regional springs (solid blue diamonds) for the period Oct. 2013–Dec. 2015. (B) Seasonal overall averages of $\delta^{18}O$ and $\delta^{2}H$ for precipitation (P; solid symbols) and groundwater (GW; empty symbols). The spring, summer autumn and winter values are indicated by green circles, red triangles, blue squares and orange diamonds, respectively. GMWL (Clark and Fritz, 1997) is the Global Meteoric Water Line (slope 8 and *dex* = 10‰), WMMWL is the Western Mediterranean Meteoric Water Line (slope 8 and *dex* = 14‰) and LMWL is the Local Meteoric water Line (slope 8,05 and *dex* = 12,74‰). (For interpretation of the references to colour in this figure legend, the reader is referred to the web version of this article.)

lowing a certain seasonal pattern (Schotterer et al., 1993; Liu et al., 2008; Froehlich et al., 2008). The lack of such seasonal pattern supports the Mediterranean as the main rainfall source.

A sine-wave function [Eq. (1)] is used to characterize every one of the measured seasonal time series of isotopic content in water from the sampling points (Fig. B1 in Appendix B). Tables 2 and 3 show the calibrated mean isotopic content ($\overline{\delta}$) and amplitude (A) corresponding to the time series of isotopic content of precipitation and spring discharge, respectively.

The mean isotopic content in rainfall $\overline{\delta}_{in}$ shows a clear-cut linear relationship with elevation (Fig. 6) that allows defining Isotopic Altitudinal Lines (IAL) for $\delta^{18}O$, $\delta^{2}H$ and *dex*, with slopes (i.e., vertical gradients $\nabla_z\delta^{18}O$, $\nabla_z\delta^{2}H$ and $\nabla_z dex$) of −1,9, −12,1 and 4,7 ‰/km, respectively. Vertical gradients ($\nabla_z\delta$) of mean isotopic content in precipitation are common in mountain zones (see Poage and Chamberlain, 2001, and references therein) and are related to the atmospheric decreasing thermal vertical profile existing along the slope of the mountains. $\nabla_z\delta$ values obtained for the study zone are like those obtained in other alpine areas, especially in the central Pyrenees and the Alps (Table 4).

The vertical gradients of the mean isotopic content in precipitation depend linearly on the mean seasonal precipitation (Fig. 7). In the case of $\delta^{18}O$ and $\delta^{2}H$, the higher the seasonal precipitation is, the lower the seasonal gradient is. In the case of *dex*, the relationship is reversed, obtaining a higher $\nabla_z dex$ value as seasonal precipitation increases. In a seasonal framework, recycling moisture evaporated from the land surface to atmosphere may increase *dex* of local precipitation. Soil evaporation is maximum when atmospheric vapor pressure

Table 2
Mean value $\overline{\delta}_{in}$ and amplitude $A_{\delta_{in}}$ of the seasonal variation in the isotopic content of precipitation for the sampled pluviometers.

	$\overline{\delta}_{in}$ (‰)			$A_{\delta_{in}}$(‰)	
Pluviometer	$\delta^{18}O$	$\delta^{2}H$	*dex*	$\delta^{18}O$	$\delta^{2}H$
P-01	−9.20	−59.91	14.56	3.34	26.89
P-02	−9.50	−62.29	13.88	2.87	23.23
P-03	−9.20	−60.25	12.94	3.29	27.92
P-04	−8.60	−56.11	12.87	3.02	26.05
P-05	−8.60	−55.65	12.37	3.05	23.31
P-06	−7.80	−51.10	9.53	2.76	23.96
P-07	−7.50	−49.06	10.24	2.59	20.92
P-08	−7.50	−50.22	9.40	2.55	19.53

Table 3
Mean value $\overline{\delta}_{out}$ and amplitude $A_{\delta_{out}}$ of the seasonal variation in the isotopic content of groundwater for the springs sampled. For every spring, the elevation of the corresponding recharge zone Z_R is included. For this elevation, the associated amplitude $A_{\delta_{ZR}}$ of the seasonal variation in isotopic content of precipitation is shown.

	$\overline{\delta}_{out}$ (‰)			$A_{\delta_{out}}$(‰)		Z_R (m a.s.l)			$A_{\delta_{ZR}}$(‰)	
Spring	$\delta^{18}O$	$\delta^{2}H$	*dex*	$\delta^{18}O$	$\delta^{2}H$	$\delta^{18}O$	$\delta^{2}H$	*dex*	$\delta^{18}O$	$\delta^{2}H$
S-01	−9,31	−60,65	13,81	0,12	1,10	1892	1881	1852	3,16	26,23
S-02	−9,61	−62,82	14,06	0,25	1,93	2038	2046	1902	3,24	27,18
S-03	−9,18	−59,85	13,60	0,11	1,07	1830	1819	1702	3,12	25,88
S-04	−9,01	−58,11	13,95	0,10	0,67	1745	1686	1881	3,07	25,12
S-05	−9,73	−63,36	14,50	0,14	0,88	2099	2088	1994	3,28	27,41
S-06	−9,69	−64,03	14,80	0,15	0,90	2078	2140	1798	3,27	27,71
M-05	−9,01	−58,53	13,52	0,44	1,81	1744	1718	1793	3,07	25,31
M-06	−8,70	−54,75	14,88	0,54	2,51	1597	1428	2071	2,98	23,65
M-08	−9,49	−62,22	13,68	0,27	1,84	1979	2001	1826	3,21	26,92
M-14	−9,69	−64,01	13,53	1,08	8,01	2079	2138	1795	3,27	27,70
M-15	−9,73	−63,81	14,05	0,87	6,24	2099	2123	1901	3,28	27,61
M-16	−9,77	−64,13	14,05	0,65	4,00	2118	2147	1902	3,29	27,75
M-17	−9,76	−64,32	13,73	0,49	2,86	2110	2161	1836	3,29	27,83
M-18	−9,59	−63,12	13,64	0,62	4,12	2031	2070	1817	3,24	27,31
M-24	−9,41	−62,26	13,02	0,47	1,64	1941	2004	1690	3,19	26,93
M-35	−8,90	−57,02	14,14	0,94	7,54	1690	1602	1920	3,04	24,65
M-37	−8,44	−54,00	13,53	0,26	0,93	1469	1371	1795	2,90	23,33

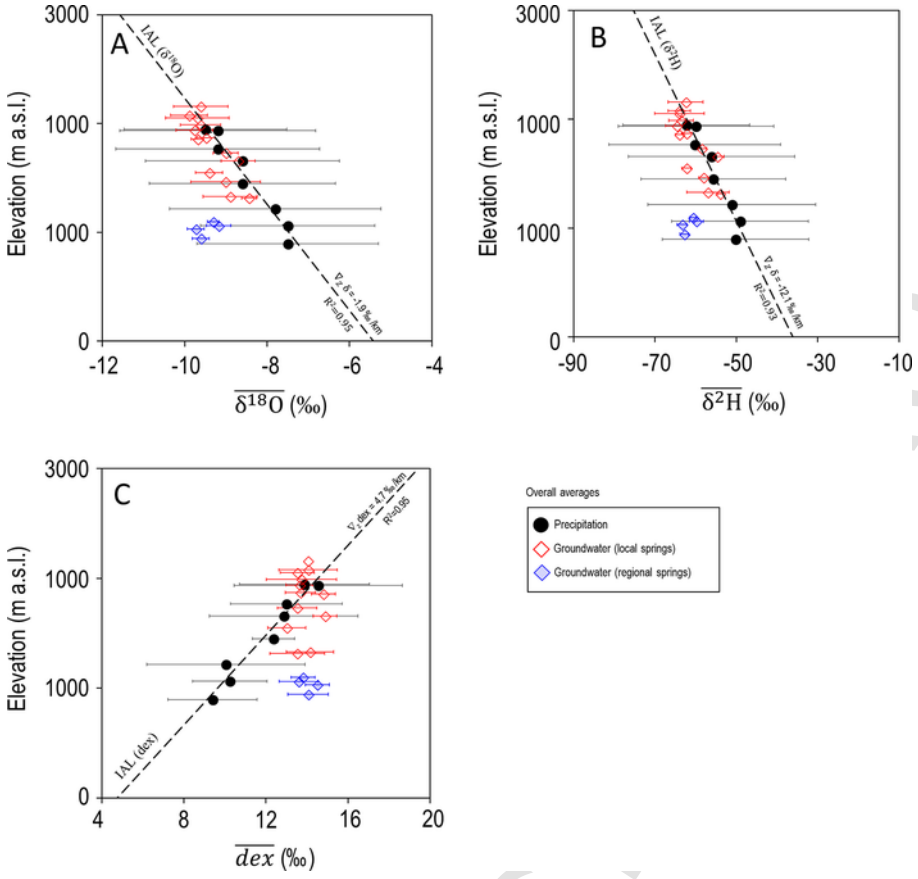

Fig. 6. Relationship between elevation and the mean isotopic content in precipitation and springs. (A) $\delta^{18}O$, (B) $\delta^{2}H$, and (C) *dex*. Error bars indicate the standard deviation. Dashed lines indicate the local Isotopic Altitudinal Line (IAL) of precipitation.

Table 4
Vertical gradients of mean isotopic water content and amplitude of the seasonal variation of the isotopic water content in precipitation.

Zone	Z_{min}–Z_{max} (m a.s.l.)	$\nabla_z\delta^{18}O$ (‰/km)	$\nabla_z\delta^{2}H$ (‰/km)	$\nabla_z dex$ (‰/km)	$\nabla_z A_{\delta^{18}O}$ (‰/km)	$\nabla_z A_{\delta^{2}H}$ (‰/km)	Reference
Eastern Pyrenees (PCM[a])	896–1936	−1,9	−15,2	4,7	0,6	6,1	This study
Central Pyrenees (PNOMP[b])	772–2200	−2,2	−17,4	2,2	0,9	4,4	Jódar et al. (2016a)
Bernese Alps	874–2023	−3,0	−19,7	3,7	1,6	14,6	Jódar et al. (2016b)
Austrian Alps	580–2245	−1,9	−12,0	2,7	–	–	Froehlich et al. (2008)
Austrian Alps	469–1598	−1,3	−8,0	3,4	–	–	Froehlich et al. (2008)
Central Andes (western flank)	2380–4250	−4,7	−42,5	2,2	–	–	Aravena et al. (1989)
Central Andes (eastern flank)	2380–4250	−1,9	−14,3	1,1	–	–	Fiorella et al. (2015)
Central Andes (eastern flank)	200–4080	−1,7	−11,7	2,0	–	–	Gonfiantini et al. (2001)
Western Carpathians	104–2008	−2,1	–	–	–	–	Holko et al. (2012)
Mount Cameroon	10–4050	−1,16	−11,4	1,4	–	–	Gonfiantini et al. (2001)

[a] Port del Comte Massif.

[b] Ordesa and Monte Perdido National Park.

deficit ($\Delta e = e - e_{sat}$, e being the atmospheric water pressure and e_{sat} the saturating water pressure at the air parcel temperature) is maximum, if the soil contains water for evaporating. Therefore, to allow soil water to evaporate, it is necessary to have enough (1) soil water content, which is higher in spring and autumn since these are the rainiest seasons, and (2) atmospheric vapor pressure deficits (Δe). Satisfying these two conditions, $\nabla_z dex$ is maximum when the difference in *dex* (i.e., Δe) between the highest and the lowest points of the mountain slope is maximum. Given that e_{sat} is an increasing function of temperature (Gonfiantini et al., 2001), Δe will decrease as temperature declines. During the cold season, despite a thermal difference existing between the highest and lowest points of the mountain, the difference in Δe between these points is minimum. Additionally, the commented Δe difference is minimum as well when there is no thermal difference along the mountain slope, a situation that is favored by the cathabaltic winds in winter (Obleitner, 1994; Gladich et al., 2011) but is also favored by the vertical atmosphere air mixing during the typical summer local low pressure convective rainfall events.

The amplitude of the seasonal variation in the isotopic content of precipitation $A_{\delta_{ip}}$ relates linearly to elevation (Fig. 8) to allow defining Amplitude Altitudinal Lines (AAL) for $\delta^{18}O$ and $\delta^{2}H$ with slopes (i.e., vertical gradients $\nabla_z A_{\delta^{18}O}$ and $\nabla_z A_{\delta^{2}H}$) of 0,6 and 5,7‰/km, respectively. Similar vertical gradients have previously been reported

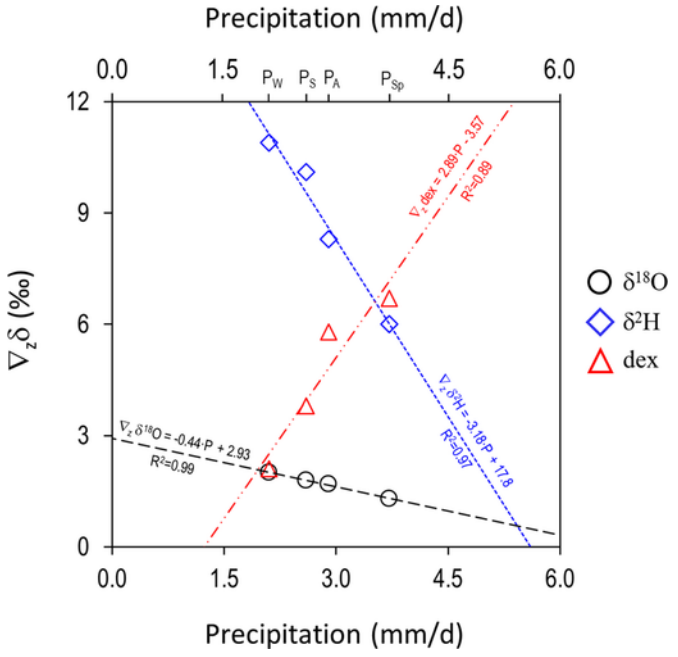

Fig. 7. Dependence of the vertical gradient of the mean isotopic content with respect to the mean seasonal precipitation. The subscripts Sp, S, A, and W stand for spring, summer, autumn and winter, respectively.

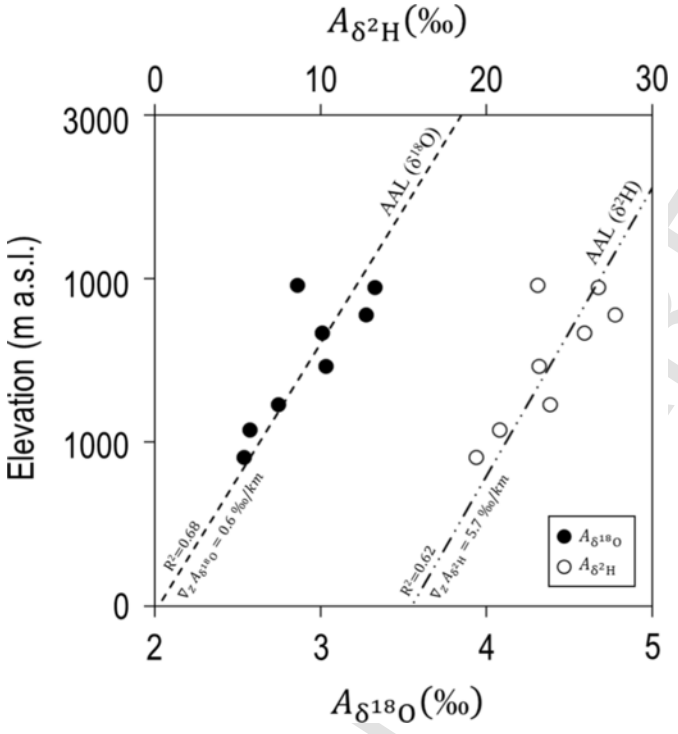

Fig. 8. Relationship between elevation and amplitude of the seasonal variation of the isotopic content ($\delta^{18}O$, δ^2H) in precipitation. Dashed line and dashed-dotted line indicate the local Amplitude Altitudinal Lines (AALs) of precipitation for $\delta^{18}O$ and δ^2H, respectively.

in the central Pyrenees (Jódar et al., 2016b) and the Bernese Alps (Jódar et al., 2016a) (Table 4).

The mean isotopic content of groundwater corresponding to local (perched) springs shows a relationship with elevation dependence with a vertical gradient larger than that of precipitation (Fig. 6), indicating the existence of aquifer recharge along the mountain slope, a process also known as slope effect (Custodio and Jódar, 2016). Additionally, the evolution of the isotopic content in the spring discharge shows a seasonal dependence like precipitation but showing smaller amplitudes (Fig. B1 in Appendix B). Even being lumped, the seasonal pattern of recharge is observed in the spring discharge, indicating that MTT should not be longer than 5 or 6 years (De Walle et al., 1997).

The isotopic altitudinal line (IAL, Fig. 6) allows estimation of the elevation of the recharge zone (Z_R) corresponding to every spring by projecting their mean isotopic content on IAL. Table 3 shows Z_R for all the springs, with their mean Z_R value ranging between 1420 m a.s.l. (M-37) and 2136 m a.s.l. (M-17). With a known value for Z_R, it is possible to calculate the amplitude of the variation in the isotopic content in precipitation at the recharge zone elevation ($A_{\delta_{ZR}}$) by projecting Z_R on the amplitude altitudinal line (AAL, Fig. 8). Table 2 shows $A_{\delta_{ZR}}$ for every spring. Finally, if both $A_{\delta_{ZR}}$ (i.e., $A_{\delta_{in}}$ at the springs recharge zone) and $A_{\delta_{out}}$ are known, it is possible to obtain a first analytical estimate of MTT through [Eq. (8)]. Table 5 provides the MTT values obtained for all the springs. As can be shown, the obtained MTT values range between 0,5 and 5 yr.

4.2. Aquifer recharge evaluation through HBV

The HBV semi-distributed conceptual rainfall–runoff model has been used to simulate the observed groundwater discharge in every spring. The spring discharges were measured every fortnight between July 2013 and October 2015. This period has been used for calibrating the HBV parameters, which are shown in Table C4 (Appendix C). The efficiency parameter R_{eff} that describes the goodness of the model fit ranges between 0,55 (S-01) and 0,77 (S-05) (Table C5, Appendix C). The computed discharges resemble the observed discharges by reproducing their temporal evolution in all the springs (Fig. 3).

The results from the HBV model indicated that recharge is especially concentrated in the open areas (VZ_1) and meadow areas (VZ_2). The yearly average effective recharge ranges from 210 mm/yr (S-04) to 637 mm/yr (S-06) (Table 6). The aquifer infiltration capacity ξ (i.e., the ratio between Q_{Re} – the effective recharge of the aquifer, and

Table 5
MTT values estimated for the springs sampled.

	$\delta^{18}O$			δ^2H		
Spring	τ^a(yr)	τ^b(yr)	η(−)	τ^a(yr)	τ^b(yr)	η(−)
S-01	4,10	2,25	1,02	3,78	3,00	1,01
S-02	2,06	1,42	1,02	2,23	1,96	1,00
S-03	4,67	2,25	1,00	3,83	2,33	1,01
S-04	4,70	2,33	1,01	5,93	2,67	1,00
S-05	3,73	2,88	1,02	4,98	2,83	1,01
S-06	3,47	2,58	1,02	4,90	2,75	1,02
M-05	1,10	–	1,00	2,22	–	1,00
M-06	0,86	–	1,00	1,49	–	1,00
M-08	1,89	–	1,00	2,32	–	1,00
M-14	0,45	–	1,00	0,53	–	1,00
M-15	0,58	–	1,00	0,69	–	1,00
M-16	0,79	–	1,00	1,09	–	1,00
M-17	1,06	–	1,00	1,54	–	1,00
M-18	0,82	–	1,00	1,04	–	1,00
M-24	1,07	–	1,00	2,61	–	1,00
M-35	0,49	–	1,00	0,5	–	1,00
M-37	1,77	–	1,00	3,99	–	1,00

[a] Analytical MTT value obtained by [Eq. (8)].

[b] Numerical MTT value obtained by FlowPC.

Table 6
Mean annual precipitation P_{ZR}, mean aquifer recharge Q_R, seasonal distribution of recharge, infiltration capacity ξ.

Spring	P_{ZR}	Q_R	$\frac{Q_{R_{e\ Spring}}}{Q_R}$	$\frac{Q_{R_{e\ Summer}}}{Q_R}$	$\frac{Q_{R_{e\ Autumn}}}{Q_R}$	$\frac{Q_{R_{e\ Winter}}}{Q_R}$	ξ[a]
	(mm/yr)	(mm/yr)	(%)	(%)	(%)	(%)	(%)
S-01	954	473	37,5%	15,0%	25,4%	22,1%	49,6%
S-02	1006	433	40,8%	12,3%	23,8%	23,1%	43,0%
S-03	793	227	38,1%	6,7%	27,2%	27,9%	28,6%
S-04	698	210	37,0%	10,2%	25,4%	27,4%	30,1%
S-05	1008	429	42,5%	14,3%	23,0%	20,2%	42,6%
S-06	1030	637	45,9%	8,9%	21,2%	24,0%	61,9%

[a] $\xi = Q_{R_e}/P_{ZR}$.

P_{ZR} - precipitation at the spring recharge zone) ranges as the yearly average ranges from 28,3% (S-03) to almost 62% (S-06) (Table 6).

Aquifer recharge follows a linear relationship similar to precipitation, as found by Martos-Rosillo et al. (2015) for the mountain carbonate aquifers in the Betic Cordillera (Southern Spain), where recharge is generally lower (Fig. 9A). In PCM, recharge is at a maximum in spring, accounting for 40,3% of the total recharge, and this outcome is explained by both rainfall and snow melt infiltration. Recharge is at a minimum (11,2%) in summer, coinciding with the period of minimum seasonal precipitation.

The relationship between ξ and P (Fig. 9B) is not as clear as the relationship between ξ and R (Fig. 9C), indicating that precipitation is a necessary condition for aquifer recharge, but it is not enough. In this respect, the results of the application of the linear regression model between the variables $Z_{R,}$ $P_{ZR,\ and}$ VZ_1, VZ_2 and $VZ_{3,}$ shows that the Z_R and is the most important predictor controlling the aquifer infiltration capacity ξ. In addition, VZ_1 (karren fields and sinkholes at the highest parts of the massif) and VZ_3 (forest fields at the lowest of the massif) also play a role regarding ξ. These parameters reflect the differences in both the karstification degree and the vegetation covering the epikarst system in the PCM.

4.3. Determination of spring discharge mean transit time

To estimate the mean transit time of the spring discharge, the program FlowPC v3.2 (Małoszewski and Zuber, 1996) has been used. According to the hydrogeological setting, it is assumed that the EPM flow model can describe the behavior of the aquifers discharging through the springs of PCM. The lumped model parameters (η and τ) have been calibrated (Table 5) by fitting the isotopic contents observed in the spring discharge from December 2013 to December 2015 (Fig. 10). The goodness of fit is defined in terms of RMSE, ranging between 0,02‰ (S-05) and 0,04‰ (S-02) for $\delta^{18}O$ (Table D1, Appendix D), and between 0,17‰ (S-03) and 0,22‰ (S-04) for $\delta^{2}H$ (Table D2, Appendix D).

The estimated value of η is very close to 1 regardless of the spring, indicating that the corresponding aquifers behave as almost an exponential flow model in coherence with the behavior of a karst aquifer system discharging through a main spring. The estimated MTT with the applied methodology ranges between 1,69 yr (S-02) and 2,85 yr (S-05), while in the case of the analytical approach MTT ranges between 2,14 yr (S-02) and 5,31 yr (S-04).

The MTT values obtained by this numerical approach are 1,9 times shorter than the MTT values analytically obtained through [Eq. (8)] that compares the amplitude of the seasonal isotopic content of recharge with the seasonal isotopic content in the spring discharge [Fig. 11]. In the numerical case, the monthly isotopic content in recharge is weighted by the monthly volumetric recharge rate, whereas in the analytical case, the isotopic content weighting coeffi-

Table 7
No standardized (λ) and standardized (β) regression coefficients associated with the explanatory variables used in the multiple regression method.

Explanatory variable	λ	β
Intercept (λ_0)	−39,562	–
Z_R	0,047	0,823
P_{ZR}	−0,007	−0,054
VZ_1	6034	0,133
VZ_2	4018	0,072
VZ_3	258,518	0,122

Table 8
Estimation of dynamic volume V_m stored in the aquifer for the springs analyzed.

Spring	V_m (hm^3)
S-01	2,44 + 0,49
S-02	11,54 + 2,61
S-03	1,72 + 0,04
S-04	0,03 + 0,01
S-05	19,39 + 0,20
S-06	0,09 + 0,01

Table 9
Brief summary of published research studies of groundwater flow karst systems in mountain areas with thick USZ the pan-European zone.

Code	High mountain karst system	NSZ thickness	Reference
1	Yunquera-Sierra de las Nieves	1000	Andreo et al. (2004); Pardo-Igúzquiza et al. (2015)
2	Alta Cadena	700	Mudarra and Andreo (2011)
3	Sierra Gorda	500	Mudarra and Andreo (2015)
4	Picos de Europa	1500	Ballesteros et al. (2015a); Ruiz and Poblete (2012)
5	Ordesa y Monte Perdido	1500	Lambán et al. (2015); Jódar et al. (2016b)
6	Port del Comte	1000	(This research)
7	Fontaine Vaucluse	800	Fleury et al. (2007)
8	Schlichenden Brünnen-Muotathal	1000	Jeannin (2001)
9	Wetterstein Mountains (Zugspitze)	1000	Lauber and Goldscheider (2014)
10	Wimbachtal catchment	1500	Maloszewski et al. (1992)
11	Totes Gebirge	1000	Laimer (2010)
12	Schneealpe Massif	900	Rank et al. 1992; Małoszewski and Zuber (2002)
13	Cansiglio-Cavallo karst aquifer	800	Filippini et al. (2018)
14	Mount Kanin	2000	Zini et al. (2015); Turk et al. (2015)
15	Gacka	1000	Ozyurt et al. (2014)
16	Gran Sasso aquifer	1500	Falcone et al. (2008); Amuroso et al. (2013)
17	Arabika Massif	2500	Klimchouk et al. (2009)
18	Aladaglar Mountains	2000	Ozyurt and Bayari (2008)

Table C4
Calibrated values of the parameters in the HBV-light model.

Catchment parameters	Units	S-01	S-02	S-03	S-04	S-05	S-06
Snow routine (VZ_1)							
TT	°C	-0,2	−4,52	−1,6	−1,1	−1	−1,1
CFMAX	mm/d/°C	1,9	2,4	2	1,7	2,8	1,2
SFCF	–	1	2,38	0,5	1	1,2	1,5
CFR	–	1	2,5	0,7	0,5	0,6	0,6
CWH	–	0,5	2	2	1	0,8	0,8
Snow routine (VZ_2)							
TT	°C	−0,2	−4,39	−1,6	−0,5	−3	−0,46
CFMAX	mm/d/°C	1,9	1	2	1,6	1	2,1
SFCF	–	1	2,6	0,7	1	1,2	1,16
CFR	–	1	2,5	0,7	0,3	1	1
CWH	–	1	2	1	1	0,2	0,2
Snow routine (VZ_3)							
TT	°C	4	6	6	0	5,5	6,5
CFMAX	mm/d/°C	1,5	1	1,5	1,5	1	4
SFCF	–	0,001	0,001	0,001	0,01	0,001	0,001
CFR	–	0,7	1	0,7	0,2	0,4	0,4
CWH	–	2	2	3	1	1	1
Soil moisture routine (VZ_1)							
FC	mm	95	75	80	75	50	80
LP	–	0,07	0,01	0,02	0,02	0,01	0,01
BETA	–	0,60	0,40	1,54	1,70	0,30	2,5
Soil moisture routine (VZ_2)							
FC	mm	180	120	150	125	139	150
LP	–	0,07	0,01	0,06	0,01	0,01	0,01
BETA	–	0,60	2,20	3,90	3,45	1,80	2,7
Soil moisture routine (VZ_3)							
FC	mm	750	550	490	750	660	700
LP	–	0,00	0,01	0,01	0,01	0,01	0,01
BETA	–	6,00	3,00	5,70	6,00	3,50	4,00
Response routine							
PERC	mm/d	5	20,0	2,2	1,1	25,0	1,7
UZL	mm	100	80	100	110	100	100
K0	1/d	0,20	0,50	0,20	0,20	0,20	0,40
K1	1/d	0,07	0,11	0,13	0,17	0,20	0,20
K2	1/d	0,01	0,02	0,04	0,04	0,05	0,05
Routing routine							
MAXBAS	d	1,7	6,2	2	2,45	4,3	4,22

cients for the monthly recharge are all equal to 1 because recharge is assumed constant (i.e., steady state) for the whole period covered by the isotopic content time series. This assumption is worth keeping in mind when using [Eq. (8)] for estimating groundwater mean transit times. In other words, if aquifer recharge shows a seasonal pattern, then the numerical approach should be used instead of the analytical approach to estimate MTT. The transit time discrepancies between both approaches may be critical when MTT is used as a vulnerability indicator for karst-fissure aquifers (Malík et al., 2016). The results obtained suggest that the numerical approach based explicitly on considering the recharge series in the LPM model provides a more accurate evaluation of hydraulic dynamics throughout the system. This allows better MTT estimations, similar of what concluded Vitvar et al. (1999) in pre-alpine non-karst aquifers. The MTT values obtained in this work are consistent with the conceptual model of the karst system. The aquifer presents specific zones with rapid recharge through surficial karstic elements (e.g. swallow holes) and slow recharge trough meadows and forest.

In terms of MTT, the results obtained in this study are similar to those obtained in other hydrological karst systems located in mountain zones: (1) In the case of the Ordesa and Monte Perdido karst aquifer system (Central Pyrenees, Spain), which is the highest calcareous massif in Western Europe, Lambán et al. (2015) and Jódar et al. (2016b) estimated MMT for several springs. For each spring the authors fitted a sinusoidal function [Eq. (1)] to the measured tracer ($\delta^{18}O$ and $\delta^{2}H$) content time series corresponding to rainfall entering the system as recharge and the spring discharge, obtaining the amplitude of the seasonal variation of both the input and output system tracer function ($A_{\delta_{in}}$ and $A_{\delta_{out}}$, respectively; Fig. 4). Besides, the authors assumed a constant recharge rate along the year. This hypothesis allowed obtaining an analytical solution to the convolution integral [Eq. (5)] (Jódar et al., 2014) but also applying [Eq. (8)] to directly estimate MTT, that ranged between 1,12 and 4,48 yr.

(2) In the Wimbach high-alpine karst system (Berchtesgaden Alps) Einsiedl et al. (2009) estimated MTT with FlowPC. To this end, they used as tracer input function the time series of ^{3}H content in rainfall measured in a meteorological station close to the study zone, and as system output the time series of ^{3}H content in groundwater discharge for different springs and also at the outlet of the hydrological catchment. They obtained MTT ranging between 4 and 5 yr for the considered springs, and 5 yr for the whole hydrologic catchment. For the same catchment, Maloszewski et al. (1992) evaluated the MTT by using monthly recharge time series instead of rainfall time series. The aquifer recharge time series was obtained by applying a seasonal infiltration coefficient to the observed monthly precipitation time series. With this approach they estimated a MTT of 4,15 yr. This value is close to that obtained by Einsiedl et al. (2009). Additionally, Garvelmann et al. (2017) expanded the previous studies in the Berchtesgaden Alps for a total of eight springs. For each spring they estimated MTT using two different methods; (A) by numerically solving the convolution integral [Eq. (5)], and (B) though [Eq. (8)] by previously conducting a sin-wave analysis [Eq. (1)] to the input (i.e. rainfall) and output tracer functions. The MTT obtained by both methods did not show large discrepancies for the same spring. In terms of the obtained MTT the sampled springs were be classified in two groups: a first group with relatively short MTTs (0,7 to 1,9 yr) and a second group with longer MTTs (7,3 to 12,5 yr).

(3) In the Schneealpe massif Rank et al. (1992) used the environmental tracers to study the karstic-fissured-porous aquifer system of Schneealpe, The aquifer system that is drained by two principal springs is the main drinking water resource for Vienna (Austria). It is composed of a fissured-porous aquifer with a high storage capacity that partially feds a karst aquifer conformed by a high-conductivity drainage channel network. For each aquifer they estimated MTT by calibrating a LPM with a 8 years long time series of environmental tracer data, using ^{3}H and $\delta^{18}O$ for the fissured-porous and the karst aquifer, respectively. In the former case MTTs ranged between 2,5 and 4,5 yr, whereas in the karst aquifer the estimated MTT was only 2 months. Małoszewski and Zuber (2002) recalibrated both LPMs by refining and extending up to 20 years the length of the observed time series of ^{3}H and $\delta^{18}O$ measurements. In the case of the fissured-porous aquifer the obtained MTTs ranged between 14 and 26 yr, being significantly larger than those obtained by Rank et al. (1992). Nevertheless, in the case of the karst aquifer the obtained MTTs were similar ranging between 1, 2 and 1,5 months. The large discrepancy between the MTT associated to the Fissured-Porous and karst aquifer indicates that water enters the aquifer system at the surface and flows through it towards the conductive drainage channels until reaching the springs. Nevertheless, the short MTTs associated to the karst aquifer reveal a direct hydraulic connection between the sinkholes at the surface and the drainage channel network.

(4) In the Wetterstein Mountains karst aquifer system Lauber and Goldscheider (2014) used both artificial (uranine) and environmental tracers (^{18}O and ^{2}H) to investigate the hydrological behavior of the system. Despite the low recovery of artificial tracer during the tracer test, the fast tracer arrival observed in all the sampled springs, with peak times between 1,8 and 3,2 days, indicates as in the previous case, the existence of well-developed flow paths through thick (>1000 m) USZ. This result underlines the role that may play the USZ conditioning the hydrologic response of the karst system. The authors estimated the aquifer MTT with FlowPC by using as input

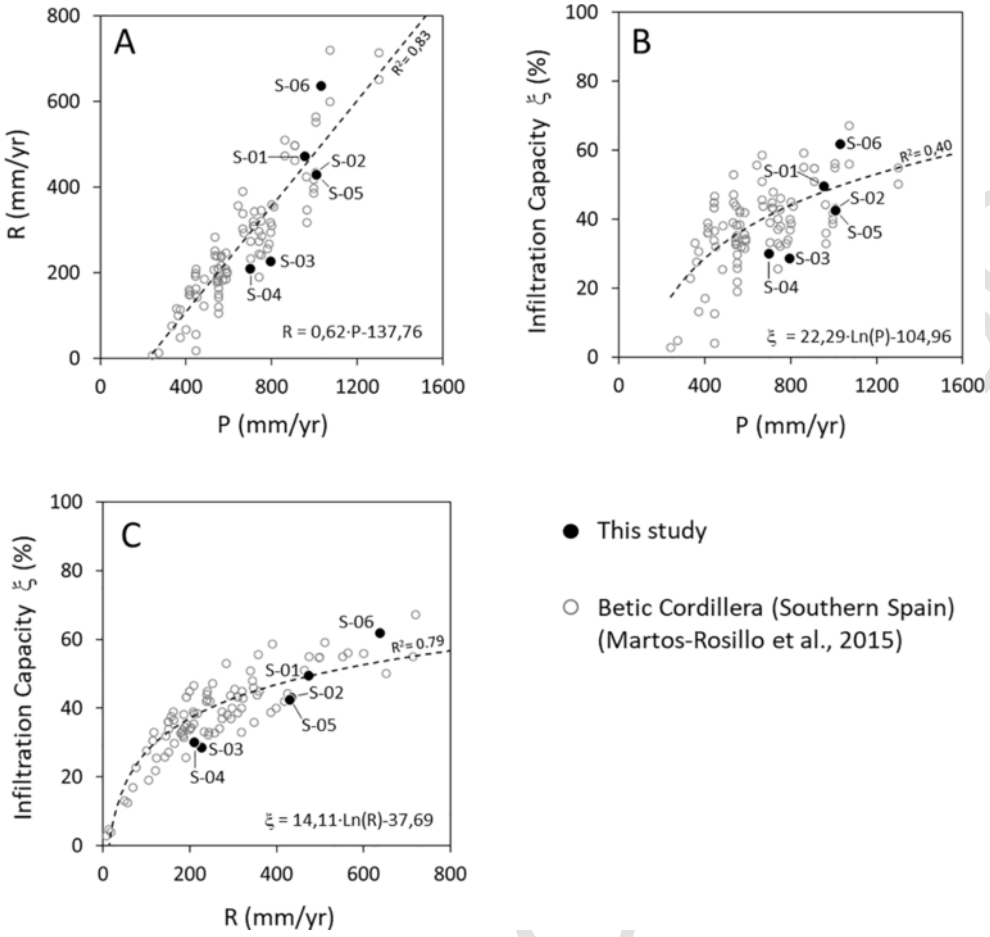

Fig. 9. (A) Mean annual rainfall versus mean annual recharge, (B) Mean infiltration coefficient versus mean annual rainfall, and (C) Mean infiltration coefficient versus mean annual recharge.

tracer content that of precipitation, and assuming a constant (without any seasonality) aquifer recharge rate. The obtained MTT values ranged between 3 and 5 months, being significantly shorter than those MTT presented above for the other karst systems.

The hydrological system MTT reflects the diversity of aquifer flow paths and groundwater mixing from the recharge zone to the discharge point. Considering that the different aquifers constituting the PCM show an exponential flow model (EM) behavior, and provided that MTT (τ; Table 5) and the aquifer mean recharge flow rate (Q_R; Table 6) are known, it is possible to estimate the aquifer storage (i.e., mixing) volume by using [Eq. (7)]. In Table 8, the stored dynamic volume ('mobile water volume - V_m'; Małoszewski and Zuber (2002); where: $V_m = Q_R \cdot \tau$) is associated with the catchment areas (Fig. A1 of the Appendix A) discharging through the springs S-01 to S-06. S-05 and S-02 play a major role in terms of both groundwater discharge and aquifer storage. The springs S-05 and S-02 present a similar area and a similar discharge. Nevertheless, from a geometrical point of view, they are different: S-05 is rounded in shape whereas S-02 is elongated. Considering that aquifer recharge is produced mainly in the highest parts of PCM, it is clear that the distance between the recharge and discharge points is larger in the case of S-02. This difference is interesting if one considers that the mean transit time of S-02 is shorter than the mean transit time of S-05. The shorter transit time would indicate a higher development of the karst water conducting features in the catchment area of S-02. The springs S-04 and S-06 denote their perched character with the associated low discharge flow rates and groundwater reserve volumes.

The few available groundwater level depth data from old water wells in the PCM suggest the karst aquifer presents low regional hydraulic gradients in the phreatic zone ranging between 1 and 2%. Nevertheless, while considering the expected mean phreatic level above the horizontal plane from the spring levels (i.e., the groundwater that contributes to each spring discharge), the 3D geological model evaluates the total aquifer formation volume (V_{aq}) associated with the regional springs S-01, S-02, S-03 and S-05. Assuming V_{aq} as known, the mean aquifer interconnected porosity (ϕ) can therefore be estimated as the ratio V_{GW}/V_{aq}. In the PCM, the average ϕ obtained is 3,1%. This result agrees with the value obtained for other carbonate aquifers of the Betic Cordillera (Southern Iberian Peninsula) with an average value of 3% (Pulido-Bosch et al., 2004; Martos-Rosillo et al., 2014).

This work is aimed to characterize the hydrological behavior of a high mountain karst system with a overlaying thick UZS that plays a relevant role along with in the system response. The applied approach allows accounting the effects of the extreme alpine climate conditions on both the aquifer recharge rates and the isotopic composition of recharge. The used approach provides a more reliable assessment of the hydrological behavior of these alpine karst systems than the obtained applying the traditional approaches found in the scarce bibliography. The methodology used in this work for characterizing the hydrological behavior of PCM can be applied in many analogue high mountain karst systems whose hydrologic behavior still remains unknown. In this sense, Table 9 shows a brief summary of the available bibliography at the pan-European zone focused on high-mountain

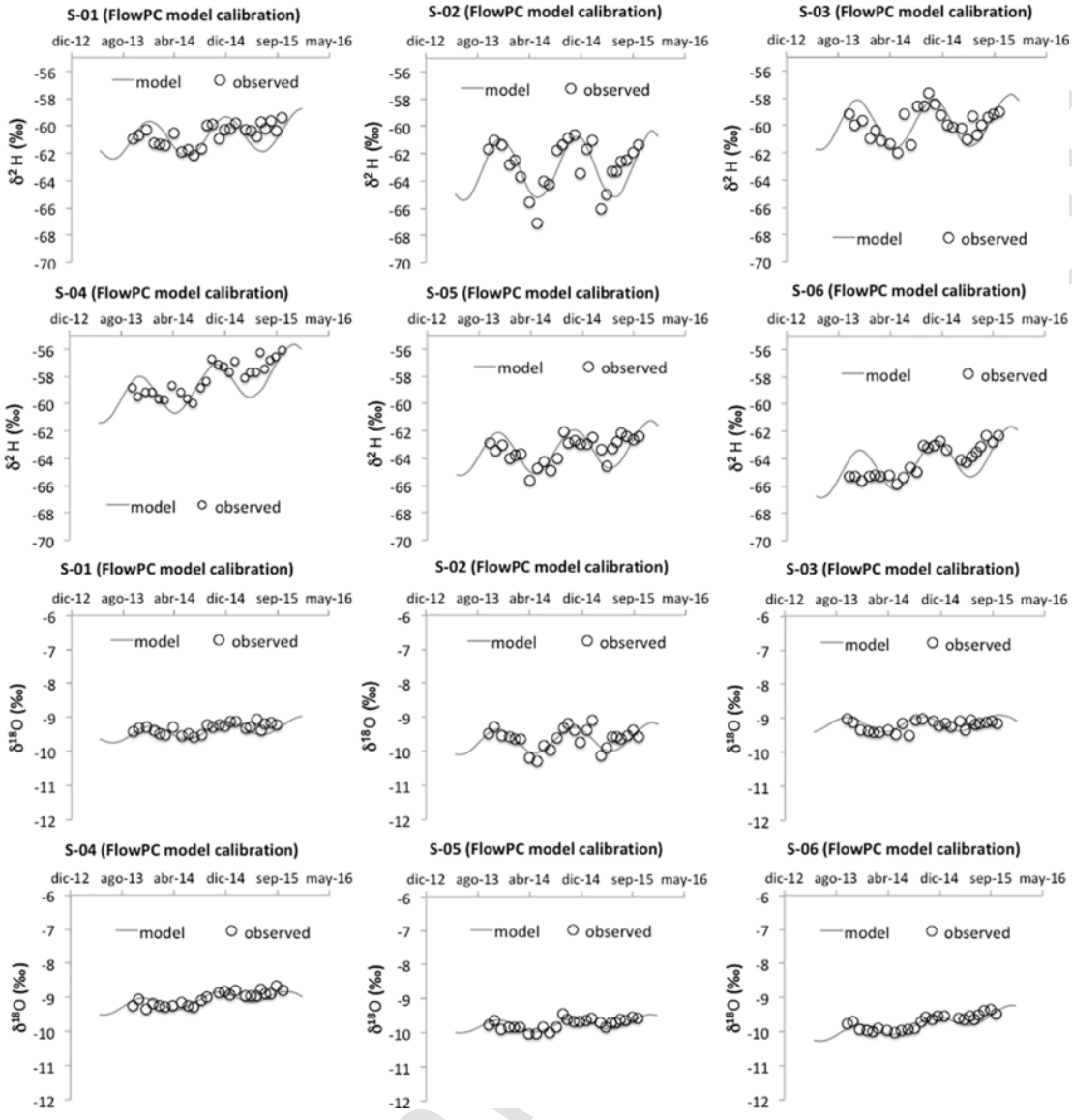

Fig. 10. Measured against simulated isotope content evolution with FlowPC and an EPM model. The gray line represents the best fit.

karst aquifers with a thick USZ in which this methodology could be tested (Fig. 12).

4.4. Evaluation of results for groundwater management purposes

MTT is a corner stone for groundwater management strategies, and many authors have used this variable as a proxy of vulnerability assessment in hydrogeological systems (Einsiedl et al. (2009) and Malík et al. (2016), among others). This work provides the first estimation of the MTT associated with most important springs discharging the PCM karst system. From the perspective of aquifer vulnerability, the intensive cattle grazing conducted in the PCM is the most threading activity to the groundwater resources stored in the underlying aquifer so far. The relatively large MTTs (2,25 yr) along with the exponential flow model describing the hydrologic behavior of PCM, points to groundwater mixing as a natural attenuation/dilution process inside the aquifer system. However, it must be taken in mind that the presence of unnoticed but likely well-developed flow paths through the USZ and also the existence of karst conductive features in the saturated zone of the PCM may favor fast contaminant migration from the recharge areas to the groundwater discharge points of this aquifer system, but this is investigation is out of the scope of this work.

From the perspective of water resources management the storage and dynamic volumes associated with the PCM aquifer system are also valuable information obtained in this study. In this line, it is worth to comment that the PCM aquifer system has an integrated groundwater storage capacity (V_{GW}) of 35,2 hm^3, and generates an overall mean annual groundwater discharge of 15,35 hm^3/yr, that represents 15% of the mean annual water consumption in the city of Barcelona (Barcelona City Council, 2018). Moreover, the average discharge of S-05, which is one of the main groundwater springs of the PCM represents 7% of the mean annual water consumption of Barcelona city. This discharge tributes to the Llobregat River Basin, which in turns provides critical water resources to the Barcelona metropolitan area. It is important keeping these numbers in mind to estimate the water resources availability given the increased frequency and severity of the Mediterranean droughts reported by the experts (Hoerling et al., 2012; Vicente-Serrano et al., 2014).

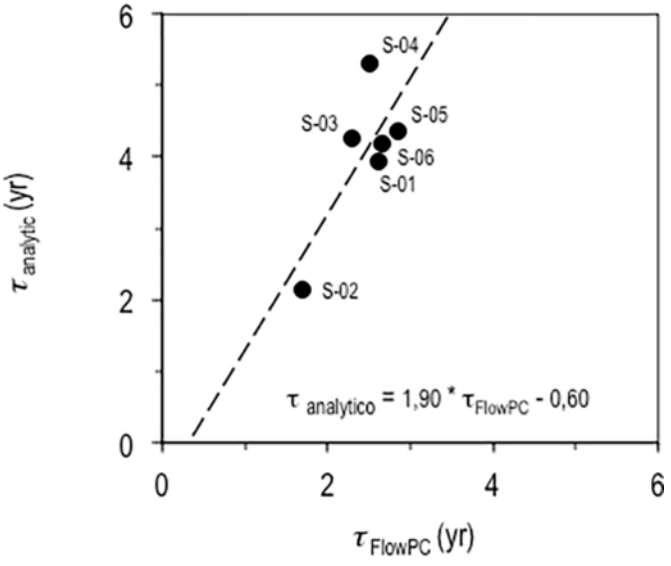

Fig. 11. Graph showing the MTT values estimated based on the lumped parameter model FlowPC (Małoszewski and Zuber, 1996) versus the MTT values estimated based on the analytical model [Eq. (8)] (Małoszewski et al., 1983).

In the Pyrenean range, climate models forecast a precipitation decrease up to 14% with respect to the observed mean precipitation and a temperature increase between 2 and 4 °C that will reduce the amount of solid precipitation and the corresponding snowmelt runoff (López-Moreno et al., 2008, 2009). In addition, the duration of the snowpack will be shorter, shifting the timing of the snowmelt (Adam et al., 2009). The PCM is in the pre-Pyrenean zone to the South of the Pyrenean axial zone. Here, the elevation of the mountains is lower, and the climate conditions are not so severe, accelerating the impact of the forecast temperature increase on snow precipitation, snowmelt runoff generation and the dynamics of the hydrological systems located in this area. Therefore, the geographical and hydrogeological settings of the PCM, along with the groundwater transit times calculated, make the PCM aquifer system an exceptional observatory for anticipating and studying the climate change impact on southern Europe. In this line, it would be extremely important to maintain the observation research program to fully understand the hydrogeological behavior of this aquifer system.

4.5. Future works in PCM

This study is the first stage in the full hydrogeological characterization of this aquifer system. The next step is to conduct the hydrogeochemical characterization of recharge and groundwater springs discharge to complement the results obtained in this work by focusing in relevant unsolved questions like (1) the role play by the epikarst zone in the total transit time of groundwater and how this role is reflected in the hydrogeochemical evolution of the springs discharge after important rainfall events and during low-flows and (2) the use of artificial tracers and environmental isotopes (e.g. 34S, 15 N) to characterize not only the mean transit time (i.e. the first moment of the transit-time distribution) but also to profile the groundwater transit-time distribution in terms of fast, intermediate and slow groundwater flows. This investigation is crucial to evaluate the aquifer vulnerability.

5. Conclusions

A distributed rainfall-runoff model and a lumped-parameter model have been combined to estimate MTT in high-mountain karst systems with an overlying thick unsaturated zone by using the stable isotopes of precipitation as environmental tracers. The presented approach accounts for the effects of the alpine climate conditions on both the aquifer recharge rates and the isotopic composition of recharge. The used approach provides a more reliable assessment of mean transit time compared to traditional methods for such alpine karst systems.

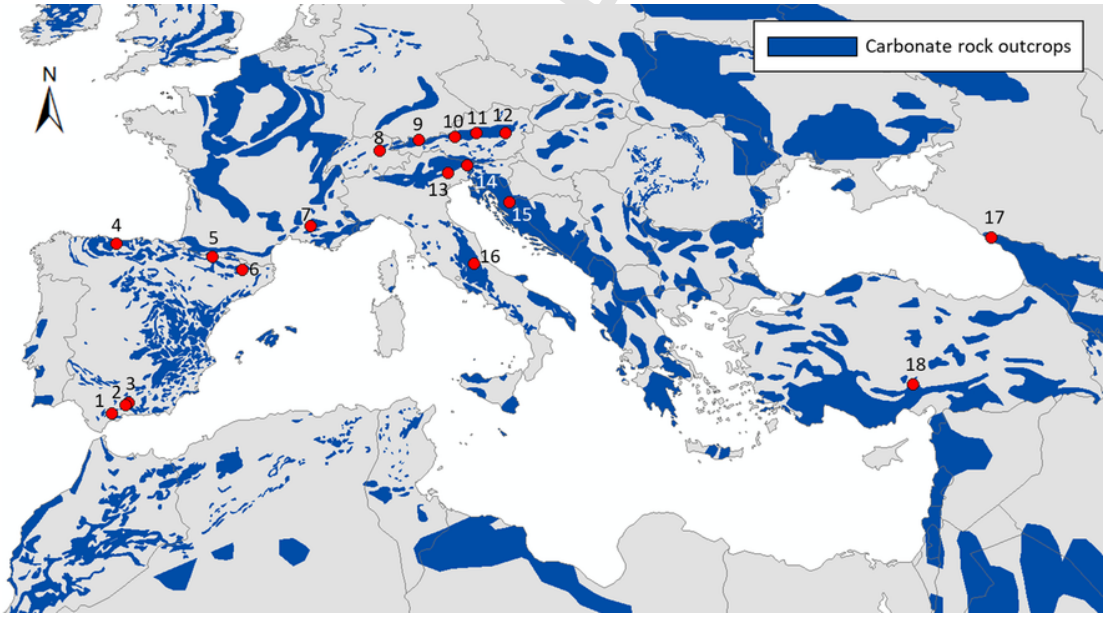

Fig. 12. Spatial distribution of carbonate rock outcrops at the pan-Mediterranean zone. Red points indicate the position of those high mountain karst aquifers zones with a thick (<500 m) NSZ referenced in the existing bibliography (map modified from the *World Map of Carbonate Rock Outcrops v.3.0*. Source: http://www.fos.auckland.ac.nz/our_research/karst). Numbers in bullets correspond to the codes shown in Table 9. (For interpretation of the references to colour in this figure legend, the reader is referred to the web version of this article.)

The approach presented in this work has been used to characterize the hydrological behavior of the Port del Comte Massif, a high mountain karst aquifer with a 1000 m thick unsaturated zone located in the southeastern part of the Pyrenees. The percentage of precipitation that enters into the hydrogeological system as aquifer recharge reaches 61,9% (the highest studied spring in the area). This elevated infiltration capacity is controlled by the presence of karren fields and sinkholes at the highest parts of Port del Comte Massif, at elevations between 2050 and 2300 m a.s.l. The evolution of the isotopic content in the sampled springs shows a sinusoidal pattern that reflects the seasonal variation of the isotopic composition of recharge. This is consistent with the relatively short groundwater transit times (2,25 yr) obtained for the hydrological system, which is in agreement with its karstic nature of the aquifer system, and emphasizes the high vulnerability of the aquifer system to variations in recharge.

The mean annual groundwater discharge and the mean water storage of the Port del Comte Massif hydrogeological system represent 16 and 34% of the mean annual water consumption in the city of Barcelona, underlying the important role as a strategic water resource that the Port del Comte Massif may play for stakeholders and water resources managers when facing the drought episodes that the Mediterranean region iteratively suffers. Moreover, given the geographical position of the study zone, located to the south of the Pyrenean axial zone, and the hydrogeological settings of the associated karst aquifer system, the Port del Comte Massif is an exceptional watchtower for anticipating the impact of climate change in Southern Europe.

Uncited references

Acknowledgments

This research was supported by Agencia Estatal de Investigación (AEI) from the Spanish Government and the European Regional Development Fund (FEDER) from EU, REMEDIATION (CGL2014-57215-C4-1-R), and PACE-ISOTEC (CGL2017-87216-C4-1-R) projects, the PIRAGUA project (EFA210/16/PIRAGUA) which is funded by the European Union through the Interreg-POCTEFA territorial cooperation program, the Catalan Government projects to support consolidated research groups MAG (Mineralogia Aplicada, Geoquimica i Geomicrobiologia, 2017SGR-1733) from Universitat de Barcelona (UB) and GREM (Grup de Recerca de Minería Sostenible) from the Universitat Politècnica de Catalunya (UPC), and the Junta de Andalucía research group RNM-308 (Hydrogeology Group). We also thank the Institut Cartogràfic i Geològic de Catalunya (Hydrogeology and Geothermics Team) and CCiT from the Universitat de Barcelona (UB) for their technical assistance, and especially Raul Carrey from the MAiMA group for the help in the laboratory analyses. The Meteorological Service of Catalonia (SMC) has kindly provided the meteorological data. The constructive comments and interesting suggestions from four anonymous reviewers are greatly appreciated since they have led to a substantial improvement of the final article.

Appendix A. Groundwater catchment areas for the springs S-01 to S-06

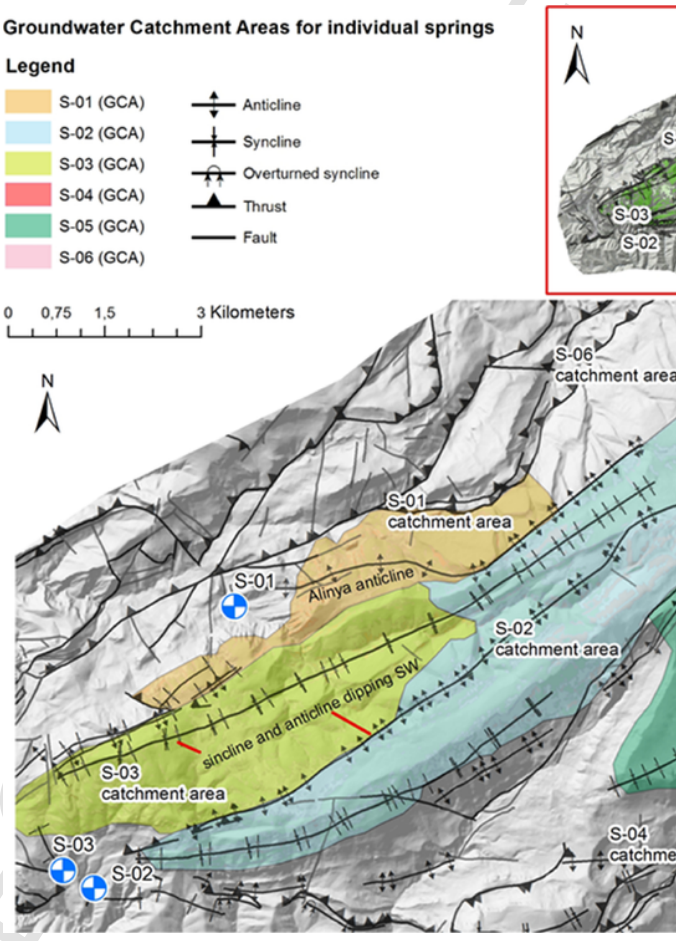

Fig. A1. Groundwater catchment areas for the springs S-01 to S-06.

Table A1 Distribution of geographical and elevation zones considered into the HBV semi-distributed rainfall-runoff model into the groundwater catchment zones. The areas of the different vegetation zones (VZs) are provided, considering the three different elevation zones into which every GWC is divided.

GWC		Elevation zones			Vegetation zone areas		
Index	Associated Spring	Z_{min} (m a.s.l.)	Z_{max} (m a.s.l.)	EZ_{ij}[a] (ha)	VZ_1[b] (ha)	VZ_2[c] (ha)	VZ_3[d] (ha)
1	S-01	1334	1600	204,0	41,8	56,8	105,5
		1601	1851	219,1	19,0	67,7	132,4
		1851	2141	122,8	4,8	6,8	111,1
2	S-02	1122	1543	106,9	8,2	26,0	72,7
		1544	1965	756,5	32,2	210,3	514,0
		1966	2385	1389,5	183,8	443,5	762,2
3	S-03	1201	1443	102,3	1,7	36,9	63,7
		1444	1686	561,2	19,5	178,9	362,8
		1687	1927	522,6	12,6	119,4	390,6
4	S-04	1468	1710	9,1	0,1	2,8	6,2
		1711	1847	0,9	0,1	0,5	0,3
		1848	1875	0,1	0,0	0,1	0,0
5	S-05	1421	1663	234,3	8,1	24,4	201,8

		1664	1973	635,5	45,4	126,0	464,1
		1974	2348	1278,4	215,5	495,0	568,0
6	S-06	1838	1926	11,9	0,7	0,7	10,5
		1927	2014	20,7	0,1	1,8	18,8
		2015	2101	13,4	0,0	2,3	11,2

[a] For a given elevation zone EZ_{ij} the subscripts "i" (from 1 to 6) and "j" refer to the corresponding groundwater catchment zone and elevation zone number, respectively.
[b] VZ_1 corresponds to open areas.
[c] VZ_2 corresponds to mountain meadows.
[d] VZ_3 corresponds to forest zones.

Appendix B. Sinusoidal functions fitting the measuring the isotopic content ($\delta^{18}O$ and $\delta^{2}H$) variation in precipitation and spring discharges

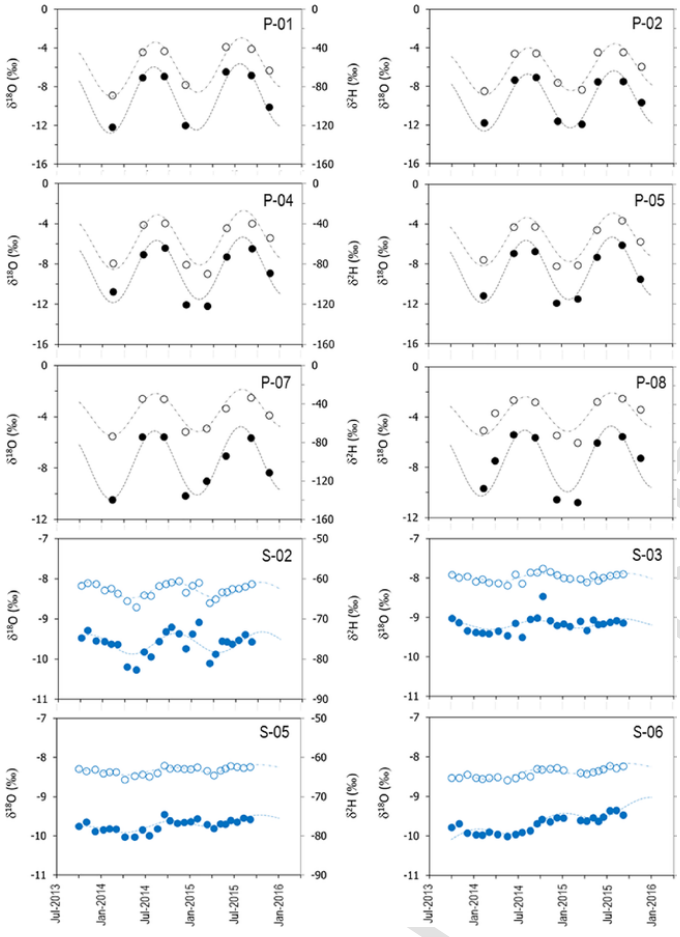

Fig. B1. Isotopic content of precipitation (P; black symbols) and spring discharge (GW; blue symbols). $\delta^{18}O$ and $\delta^{2}H$ are indicated by solid and empty symbols, respectively The dashed lines indicate the fitted sinusoidal function [Eq. (1)]. The identification codes correspond to those in Table 1. (For interpretation of the references to colour in this figure legend, the reader is referred to the web version of this article.)

Appendix C. HBV hydrological modeling

Table C1 List of abbreviations for the vegetation zone parameters of HBV (Seibert, 2005).

Parameter	Units	Valid range	Description
TT	°C	(−inf,inf)	Threshold temperature to produce accumulation of precipitation as snow. Melt of snow starts if temperatures are above TT calculated with a simple degree-day (degree-Δt in case of a non-daily time step) method
CFMAX	mm/Δt/°C	[0,inf)	Degree-Δt factor - CFMAX varies normally between 1.5 and 4 mm oC-1 day-1 (in Sweden), with lower values for forested areas. As approximation the values 2 and 3.5 can be used for CFMAX in forested and open landscape respectively.
SFCF	–	[0,inf)	Snowfall correction factor
CFR	–	[0,inf)	Refreezing coefficient
CWH	–	[0,inf)	Water holding capacity, according to: refreezing meltwater = CFR·CFMAX(TT-T)′
FC	mm	(0,inf)	Maximum soil moisture storage
LP	–	[0,1)	Soil moisture value above which AET reaches PET
BETA	–		Parameter that determines the relative contribution to runoff from rain or snowmelt

Table C2 List of abbreviations for the catchment parameters of HBV (Seibert, 2005).

Parameter	Units	Valid range	Description
PERC	mm/Δt	[0,inf)	Threshold parameter
UZL	mm	[0,inf)	Threshold parameter
K0	1/Δt	[0,1)	Storage (or recession) coefficient 0
K1	1/Δt	[0,1)	Storage (or recession) coefficient 1
K2	1/Δt	[0,1)	Storage (or recession) coefficient 2
MAXBAS	Δt	[1,100]	Length of triangular weighting function

Table C3 Objective functions for the calibration of the HBV hydrologic model, where Q_{obs_i} and Q_{sim_i} are the measured and computed of spring discharge values, respectively, $\overline{Q_{obs}}$ is the arithmetic mean of the observed spring discharge values, and $\overline{Q_{sim}}$ is the arithmetic mean of the computed spring discharge values.

Objective function	Observations
$R_{eff} = 1 - \frac{\sum_{i=1}^{N}\left(Q_{sim_i}-Q_{obs_i}\right)^2}{\sum_{i=1}^{N}\left(Q_{obs_i}-\overline{Q_{obs}}\right)^2}$	$R_{eff}=1$ means perfect fit $R_{eff}=0$, indicates that the model fits the observed data no better than a horizontal line through $\overline{Q_{obs}}$ $R_{eff}<0$ means very poor fit
$R^2 = \frac{\left(\sum_{i=1}^{N}\left(Q_{obs_i}-\overline{Q_{obs}}\right)*\left(Q_{sim_i}-\overline{Q_{sim}}\right)\right)^2}{\sum_{i=1}^{N}\left(Q_{obs_i}-\overline{Q_{obs}}\right)^2 * \sum_{i=1}^{N}\left(Q_{sim_i}-\overline{Q_{sim}}\right)^2}$	R^2 is the determination coefficient. The higher the R^2 value the better the model performance

Table C5 Goodness of the result of the HBV calibrations for each spring model.

HBV model	R_{eff} (−)	R^2 (−)
S-01	0,55	0,55
S-02	0,66	0,67
S-03	0,73	0,78
S-04	0,57	0,73
S-05	0,77	0,80
S-06	0,62	0,66

Appendix D. FlowPC modeling

Table D1 Fitted parameters of the exponential-piston flow model (EPM) for the estimated mean transit times (τ) with FlowPC model and $\delta^{18}O$ data.

Parameters	S-01	S-02	S-03	S-04	S-05	S-06
β (%)[a]	0	0	0	0	0	0
δ_β (‰)[b]	0	0	0	0	0	0
η (−)[c]	1,02	1,02	1,00	1,01	1,02	1,02
τ (yr)	2,25	1,42	2,25	2,33	2,88	2,58
RMSE (‰)	0,03	0,04	0,03	0,03	0,02	0,03

[a] A constant discharge component as a fraction (usually older) of the total spring volumetric discharge flow rate.

[b] Constant isotopic content of β.

[c] η is the ratio of the total volume to the volume with exponential distribution transit time (TTD). $\eta = 1$ means the Exponential model (EM) and $\eta > 1$ for Exponential-piston flow model (EPM)

Table D2 Fitted parameters of the exponential-piston flow model (EPM) for the estimated mean transit times (τ) with FlowPC model and δ^2H data.

Parameters	S-01	S-02	S-03	S-04	S-05	S-06
β (%)[a]	0	0	0	0	0	0
δ_β (‰)[b]	0	0	0	0	0	0
η (−)[c]	1,01	1,00	1,01	1,00	1,01	1,02
τ (yr)	3,00	1,92	2,33	2,67	2,83	2,75
RMSE (‰)	0,19	0,21	0,17	0,22	0,18	0,20

[a] A constant discharge component as a fraction (usually older) of the total spring volumetric discharge flow rate.

[b] Constant isotopic content of β.

[c] η is the ratio of the total volume to the volume with exponential distribution transit time (TTD). $\eta = 1$ means the Exponential model (EM) and $\eta > 1$ for Exponential-piston flow model (EPM).

Appendix E. Supplementary data

Supplementary data to this article can be found online at https://doi.org/10.1016/j.scitotenv.2018.11.188.

References

Adam, J.C., Hamlet, A.F., Lettenmaier, D.P., 2009. Implications of global climate change for snowmelt hydrology in the twenty-first century. Hydrological Processes: An International Journal 23 (7), 962–972. https://doi.org/10.1002/hyp.7201.

Agencia Estatal de Meteorología de España (AEMET) and Instituto de Meteorologia – Portugal (IMA), 2011. Iberian Climate Atlas. Air Temperature and Precipitation (1971–2000). In: https://www.aemet.es/documentos/es/conocermas/publicaciones/Atlas-climatologico/Atlas.pdf.

Allocca, V., De Vita, P., Manna, F., Nimmo, J.R., 2015. Groundwater recharge assessment at local and episodic scale in a soil mantled perched karst aquifer in southern Italy. J. Hydrol. 529 (2015), 843–853. https://doi.org/10.1016/j.jhydrol.2015.08.032.

Amin, I.E., Campana, M.E., 1996. A general lumped parameter model for the interpretation of tracer data and transit time calculation in hydrologic systems. J. Hydrol. 179, 1–4):1–21. https://doi.org/10.1016/0022-1694(95)02880-3.

Andreo, B., Linan, C., Carrasco, F., De Cisneros, C.J., Caballero, F., Mudry, J., 2004. Influence of rainfall quantity on the isotopic composition (^{18}O and ^{2}H) of water in mountainous areas. Application for groundwater research in the Yunquera-Nieves karst aquifers (S Spain). Appl. Geochem. 19 (4), 561–574. https://doi.org/10.1016/j.apgeochem.2003.08.002.

Araguás-Araguás, L.J., Díaz-Teijeiro, M.F., 2005. Isotope composition of precipitation and water vapour in the Iberian Peninsula. In: Isotopic Composition of Precipitation in the Mediterranean Basin in Relation to Air Circulation Patterns and Climate. pp. 173–190, (IAEA-TECDOC-1453).

Aravena, R., Peña, H., Grilli, A., Suzuki, O., Mordeckai, M., 1989. Evolución Isotópica de las Lluvias y Origen de laS Masas de Aire en el Altiplano Chileno. Isotope Hydrology Investigations in Latín America. IAEA-TECDOC-502. IAEA, Vienna, 129–142.

Bakalowicz, M., 2005. Karst groundwater: a challenge for new resources. Hydrogeol. J. 13 (1), 148–160. https://doi.org/10.1007/s10040-004-0402-9.

Ballesteros, D., Arnauld Malard, A., Pierre-Yves Jeannin, P.-Y., Jimenez-Sanchez, M., García-Sansegundo, J., Meléndez-Asensio, M., Sendra, G., 2015. KARSYS hydrogeological 3D modeling of alpine karst aquifers developed in geologically complex areas: Picos de Europa National Park (Spain). Environ. Earth Sci. 74 (12), 7699–7714. https://doi.org/10.1007/s12665-015-4712-0.

Ballesteros, D., Jiménez-Sánchez, M., Giralt, S., García-Sansegundo, J., Meléndez-Asensio, M., 2015. A multi-method approach for speleogenetic research on alpine karst caves. Torca La Texa shaft, Picos de Europa (Spain). Geomorphology 247, 35–54.

Barberá, J.A., Jódar, J., Custodio, E., González-Ramón, A., Jiménez-Gavilán, Vadillo, I., Pedrera, A., Martos-Rosillo, S., 2018. Groundwater dynamics in a hydrologically-modified alpine watershed from an ancient managed recharge system (Sierra Nevada National Park, Southern Spain): insights from hydrogeochemical and isotopic information. Sci. Total Environ. 640–641, 874–893. https://doi.org/10.1016/j.scitotenv.2018.05.305.

Barberá, J.A., Mudarra, M., Andreo, B., De la Torre, B., 2018. Regional-scale analysis of karst underground flow deduced from tracing experiments: examples from carbonate aquifers in Màlaga province, southern Spain. Hydrogeol. J. 26 (1), 23–40. https://doi.org/10.1007/s10040-017-1638-5.

Barcelona City Council, 2018. Evolution of Water Consumption in the City of Barcelona. In: http://www.bcn.cat/estadistica/angles/dades/economia/consum/evoconsum/coev04.htm, Accessed 7 August 2018.

Barnett, T.P., Adam, J.C., Lettenmaier, D.P., 2005. Potential impacts of a warming climate on water availability in snow-dominated regions. Nature 438 (7066)https://doi.org/10.1038/nature04141.

Bergström, S., 1976. Development and Application of a Conceptual Runoff Model For Scandinavian Catchments, SMHI, Report No. RHO 7 (134 pp Norrköping).

Braun, L.N., Renner, C.B., 1992. Application of a conceptual runoff model in different physiographic regions of Switzerland. Hydrol. Sci. J. 37 (3), 217–231. https://doi.org/10.1080/02626669209492583.

Butscher, C., Huggenberger, P., 2007. Implications for karst hydrology from 3D geological modeling using the aquifer base gradient approach. J. Hydrol. 342 (1–2), 184–198. https://doi.org/10.1016/j.jhydrol.2007.05.025.

Celle-Jeanton, H., Travi, Y., Blavoux, B., 2001. Isotopic typology of the precipitation in the Western Mediterranean region at three different time scales. Geophys. Res. Lett. 28 (7), 1215–1218.

Cervi, F., Marcaccio, M., Petronici, F., Borgatti, L., 2014. Hydrogeological characterization of peculiar Apenninic springs. Proceedings of the International Association of Hydrological Sciences 364, 333–338.

Chen, Z., 2017. Modeling a Geologically Complex Karst Aquifer System, Hochifen-Gottesacker, Alps. PhD. Thesis Karlsruher Instituts für Technologie, Germany https://d-nb.info/1136660852/34.

Chueca, J., Julián, A., López-Moreno, J.I., 2007. Recent evolution (1981–2005) of the Maladeta glaciers, Pyrenees, Spain: extent and volume losses and their relation with climatic and topographic factors. J. Glaciol. 53 (183), 547–557. https://doi.org/10.3189/002214307784409342.

Clark, I.D., Fritz, P., 1997. Environmental Isotopes in Hydrogeology. Lewis Publishers, New York.

Coplen, 2011. Guidelines and recommended terms for expression of stable-isotope-ratio and gas-ratio measurement results. Rapid Commun. Mass Spectrom. 2011 (25), 2538–2560.

CREAF, 2009. Land Cover Map of Catalonia (MCSC) 1:250,000. 4a Edition (2009). In: http://www.creaf.uab.es/mcsc/usa/index.htm.

Custodio, E., Jódar, J., 2016. Simple solutions for steady–state diffuse recharge evaluation in sloping homogeneous unconfined aquifers by means of atmospheric tracers. J. Hydrol. https://doi.org/10.1016/j.jhydrol.2016.06.035.

Custodio, E., Llamas, M.R. (Eds.), 1976. Hidrología subterránea [Groundwater Hydrology]. 2 Vols: 1–2350. Ediciones Omega, Barcelona.

De Jong, C., Lawler, D., Essery, R., 2009. Mountain hydroclimatology and snow seasonality and hydrological change in mountain environments. Hydrol. Process. 23, 955–961. https://doi.org/10.1002/hyp.7193.

De Walle, D.R., Edwards, P.J., Swistock, B.R., Aravena, R., Drimmie, R.J., 1997. Seasonal isotope hydrology of three Appalachian forest catchments. Hydrol. Process. 11 (15), 1895–1906, (b doi:10.1002/(SICI)1099-1085(199712)11:15<1895::AID-HYP538>3.0.CO;2-#).

Einsiedl, F., 2005. Flow system dynamics and water storage of a fissured-porous karst aquifer characterized by artificial and environmental tracers. J. Hydrol. 312, 312–321. https://doi.org/10.1016/j.jhydrol.2005.03.031.

Einsiedl, F., Maloszewski, P., Stichler, W., 2009. Multiple isotope approach to the determination of the natural attenuation potential of a high-alpine karst system. J. Hydrol. 365 (2009), 113–121. https://doi.org/10.1016/j.jhydrol.2008.11.042.

Epting, J.M., Page, R., Auckenthaler, A., Huggenberger, P., 2018. Process-based monitoring and modeling of Karst springs – linking intrinsic to specific vulnerability. Sci. Total Environ. 625, 403–415. https://doi.org/10.1016/j.scitotenv.2017.12.272.

Falcone, R.A., Falgiani, A., Parisse, B., Petitta, M., Spizzico, M., Tallini, M., 2008. Chemical and isotopic ($\delta^{18}O‰$, $\delta^{2}H‰$, $\delta^{13}C‰$, ^{222}Rn) multi-tracing for groundwater conceptual model of carbonate aquifer (Gran Sasso INFN underground laboratory–central Italy). J. Hydrol. 357 (3–4), 368–388.

Farlin, J., Maloszewski, P., 2013. On the use of spring baseflow recession for a more accurate parameterization of aquifer transit time distribution functions. Hydrol. Earth Syst. Sci. 17 (5), 1825–1831. https://doi.org/10.5194/hess-17-1825-2013.

Filippini, M., Squarzoni, G., De Waele, J., Fiorucci, A., Vigna, B., Grillo, B., Riva, A., Rossetti, S., Zini, L., Casagrande, G., Stumpp, C., Gargini, A., 2018. Differentiated spring behavior under changing hydrological conditions in an alpine karst aquifer. J. Hydrol. 556, 572–584. https://doi.org/10.1016/j.jhydrol.2017.11.040.

Fiorella, R.P., Poulsen, C.J., Pillco Zolá, R.S., Barnes, J.B., Tabor, C.R., Ehlers, T.A., 2015. Spatiotemporal variability of modern precipitation $\delta^{18}O$ in the central Andes and implications for paleoclimate and paleoaltimetry estimates. J. Geophys. Res.-Atmos. 120 (10), 4630–4656. https://doi.org/10.1002/2014JD022893.

Fleury, P., Plagnes, V., Bakalowicz, M., 2007. Modelling of the functioning of karst aquifers with a reservoir model: application to Fontaine de Vaucluse (South of France). J. Hydrol. 345, 38–49. https://doi.org/10.1016/j.jhydrol.2007.07.014.

Freixes, A., 2014. Els aqüífers Càrstics dels Pirineus de Catalunya. Interès Estratègic i Sostenibilitat [The karstic aquifers of the Catalonian Pyrenees. Strategic Interest and Sustainability]. PhD. Thesis Universitat de Barcelona http://hdl.handle.net/2445/65187.

Froehlich, K., Gibson, J.J., Aggarwal, P., 2001. Deuterium excess in precipitation and its climatological significance. In: Study of Environmental Change Using Isotope Techniques. vol. 13, IAEA, pp. 54–66.

Froehlich, K., Kralik, M., Papesch, W., Rank, D., Scheifinger, H., Stichler, W., 2008. Deuterium excess in precipitation of Alpine regions–moisture recycling. Isot. Environ. Health Stud. 44 (1), 61–70. https://doi.org/10.1080/10256010801887208.

García-Ruiz, J.M., López-Moreno, J.I., Vicente-Serrano, S.M., Lasanta-Martínez, T., Beguería, S., 2011. Mediterranean water resources in a global change scenario. Earth Sci. Rev. 105 (3–4), 121–139. https://doi.org/10.1016/j.earscirev.2011.01.006.

Garvelmann, J., Warscher, M., Leonhardt, G., Franz, H., Lotz, A., Kunstman, H., 2017. Quantification and characterization of the dynamics of spring and stream water systems in the Berchtesgaden Alps with a long-term stable isotope dataset. Environ. Earth Sci. 76, 766https://doi.org/10.1007/s12665-017-7107-6.

Giorgi, F., Lionello, P., 2008. Climate change projections for the Mediterranean region. Glob. Planet. Chang. 63 (2–3), 90–104. https://doi.org/10.1016/j.gloplacha.2007.09.005.

Gladich, I., Gallai, I., Giaiotti, D.B., Stel, F., 2011. On the diurnal cycle of deep moist convection in the southern side of the Alps analysed through cloud-to-ground lightning activity. Atmos. Res. 100 (4), 371–376. https://doi.org/10.1016/j.atmosres.2010.08.026.

Goldscheider, N., 2005. Fold structure and underground drainage pattern in the alpine karst system Hochifen-Gottesacker. Eclogae Geol. Helv. 98 (1), 1–17. https://doi.org/10.1007/s00015-005-1143-z.

Goldscheider, N., 2011. Alpine Hydrogeologie [Alpine hydrogeology]. Grundwasser 16, 1. https://doi.org/10.1007/s00767-010-0157-2.

Goldscheider, N., Drew, D. (Eds.), 2007. Methods in Karst Hydrogeology. International Contributions to Hydrogeology 26. International Association of Hydrogeologists, Taylor & Francis, London, p. 264, (ISBN 978-0-415-42873-6).

Goldscheider, N., Meiman, J., Pronk, M., Smart, C., 2008. Tracer tests in karst hydrogeology and speleology. Int. J. Speleol. 37 (1), 3. https://doi.org/10.5038/1827-806X.37.1.3.

Gonfiantini, R., Roche, M.A., Olivry, J.C., Fontes, J.C., Zuppi, G.M., 2001. The altitude effect on the isotopic composition of tropical rains. Chem. Geol. 181 (1–4), 147–167. https://doi.org/10.1016/S0009-2541(01)00279-0.

Gremaud, V., Goldscheider, N., Savoy, L., Favre, G., Masson, H., 2009. Geological structure, recharge processes and underground drainage of a glacierised karst aquifer system, Tsanfleuron-Sanetsch, Swiss Alps. Hydrogeol. J. 17, 1833–1848. https://doi.org/10.1007/s10040-009-0485-4.

Grunewald, K., Scheithauer, J., 2010. Europe's southernmost glaciers: response and adaptation to climate change. J. Glaciol. 56 (195), 129–142. https://doi.org/10.3189/002214310791190947.

Hargreaves, G.H., Samani, Z.A., 1982. Estimating potential evapotranspiration. J. Irrig. Drain. Eng. 108, 223–230.

Hernández-Mora, N., del Moral Ituarte, L., La-Roca, F., La Calle, A., Schmidt, G., 2014. Interbasin water transfers in Spain: Interregional conflicts and governance responses. In: Globalized Water. Springer, Dordrecht, pp. 175–194. https://doi.org/10.1007/978-94-007-7323-3_13, ISBN 978-94-007-7322-6.

Hoerling, M., Eischeid, J., Perlwitz, J., Quan, X., Zhang, T., Pegion, P., 2012. On the increased frequency of Mediterranean drought. J. Clim. 25 (6), 2146–2161. https://doi.org/10.1175/JCLI-D-11-00296.1.

Holko, L., Dóša, M., Michalko, J., Šanda, M., 2012. Isotopes of oxygen-18 and deuterium in precipitation in Slovakia. J. Hydrosci. Hydraul. Eng. 60 (4), 265–276. https://doi.org/10.2478/v10098-012-0023-2.

Hood, J.L., Hayashi, M., 2010. Assessing the application of a laser rangefinder for determining snow depth in inaccessible alpine terrain. Hydrol. Earth Syst. Sci. 14 (6), 901. https://doi.org/10.5194/hess-14-901-2010.

Hottelet, Ch., Braun, L.N., Leibundgut, Ch., Rieg, A., 1993. Simulation of Snowpack and Discharge in an Alpine Karst Basin. IAHS Publication No. 218. 249–260.

ICGC, 2007. Mapa Geològic Comarcal de Catalunya 1:50,000. Full Alt Urgell (BDGC50M). In: http://www.icgc.cat/ca/Administracio-i-empresa/Descarregues/Cartografia-geologica-i-geotematica/Cartografia-geologica/Mapa-geologic-comarcal-de-Catalunya-1-50.000/Mapa-geologic-comarcal-de-Catalunya-1-50.000.

Jeannin, P.-Y., 2001. Modeling flow in phreatic and epiphreatic karst conduits in the Hölloch cave (Muotatal, Switzerland). Water Resour. Res. 37 (2), 191–200. https://doi.org/10.1029/2000WR900257.

Jeelani, G., Shah, R.A., Deshpande, R.D., Fryar, A.E., Perrin, J., Mukherjee, A., 2017. Distinguishing and estimating recharge to karst springs in snow and glacier dominated mountainous basins of the western Himalaya, India. J. Hydrol. 550, 239–252. https://doi.org/10.1016/j.jhydrol.2017.05.001.

Jiménez-Martínez, J., Custodio, E., 2008. El exceso de deuterio en la lluvia y en la recarga a los acuíferos en el área circum-mediterránea y en la costa mediterránea española. Bol. Geol. Min. 119 (1), 21–32.

Jódar, J., Cabrera, J.A., Martos-Rosillo, S., Ruiz-Constan, A., Gonzalez-Ramón, A., Lambán, L.J., Herrera, C., Custodio, E., 2017. Groundwater discharge in high-mountain watersheds: a valuable resource for downstream semi-arid zones. The case of the Bérchules River in Sierra Nevada (Southern Spain). Sci. Total Environ. https://doi.org/10.1016/j.scitotenv.2017.03.190.

Jódar, J., Carpintero, E., Martos-Rosillo, S., Ruiz-Constán, A., Marín-Lechado, C., Cabrera-Arrabal, J.A., Navarrete-Mazariego, E., González-Ramón, A., Lambán, L.J., Herrera, C., González-Dugo, M.P., 2018. Combination of lumped hydrological and remote-sensing models to evaluate water resources in a semi-arid high altitude ungauged watershed of Sierra Nevada (Southern Spain). Sci. Total Environ. 625, 285–300 https://doi-org.recursos.biblioteca.upc.edu/10.1016/j.scitotenv.2017.12.300.

Jódar, J., Custodio, E., Lambán, L.J., Martos-Rosillo, S., Herrera-Lameli, C., Sapriza-Azuri, G., 2016. Vertical variation in the amplitude of the seasonal isotopic content of rainfall as a tool to jointly estimate the groundwater recharge zone and transit times in the Ordesa and Monte Perdido National Park aquifer system, north-eastern Spain. Sci. Total Environ. 573, 505–517. https://doi.org/10.1016/j.scitotenv.2016.08.117.

Jódar, J., Custodio, E., Liotta, M., Lambán, L.J., Herrera, C., Martos-Rosillo, S., Sapriza, G., Rigo, T., 2016. Correlation of the seasonal isotopic amplitude of precipitation with annual evaporation and altitude in alpine regions. Sci. Total Environ. 550, 27–37. https://doi.org/10.1016/j.scitotenv.2015.12.034.

Jódar, J., Lambán, L.J., Medina, A., Custodio, E., 2014. Exact analytical solution of the convolution integral for classical hydrogeological lumped-parameter models and typical input tracer functions in natural gradient systems. J. Hydrol. 519, 3275–3289. https://doi.org/10.1016/j.jhydrol.2014.10.027.

Katsuyama, M., Tani, M., Nishimoto, S., 2010. Connection between streamwater mean residence time and bedrock groundwater recharge/discharge dynamics in weathered granite catchments. Hydrol. Process. 24 (16), 2287–2299. https://doi.org/10.1002/hyp.7741.

Kazakis, N., Chalikakis, K., Mazzilli, M., Ollivier, C., Manakos, A., Voudouris, K., 2018. Management and research strategies of karst aquifers in Greece: literature overview and exemplification based on hydrodynamic modelling and vulnerability assessment of a strategic karst aquifer. Sci. Total Environ. 643, 592–609. https://doi.org/10.1016/j.scitotenv.2018.06.184.

Klimchouk, A., Samokhin, G.V., Kasian, Y.M., 2009. The Deepest Cave in the World in the Arabika Massif (western caucasus) and its Hydrogeological and Paleogeographic Significance. 2009 ICS Proceedings. 15th International Congress of Speleology

Konz, M., Seibert, J., 2010. On the value of glacier mass balances for hydrological model calibration. J. Hydrol. 385 (1–4), 238–246. https://doi.org/10.1016/j.jhydrol.2010.02.025.

Kurylyk, B.L., Hayashi, M., 2017. Inferring hydraulic properties of alpine aquifers from the propagation of diurnal snowmelt signals. Water Resour. Res. https://doi.org/10.1002/2016WR019651.

Laimer, H.J., 2010. Neue Ergebnisse zur Karsthydrogeologie des westlichen Toten Gebirges (Österreich). (New karst hydrogeological research in the western Totes Gebirge, Austria). Grundwasser 15 (2), 113–122.

Lambán, L.J., Jódar, J., Custodio, E., Soler, A., Sapriza, G., Soto, R., 2015. Isotopic and hydrogeochemical characterization of high-altitude karst aquifers in complex geological settings. The Ordesa and Monte Perdido National Park (Northern Spain) case study. Sci. Total Environ. 506–507, 466–479. https://doi.org/10.1016/j.scitotenv.2014.11.030.

Lauber, U., Goldscheider, N., 2014. Use of artificial and natural tracers to assess groundwater transit-time distribution and flow systems in a high-alpine karst system (Wetterstein Mountains, Germany). Hydrogeol. J. 22 (8), 1807–1824. https://doi.org/10.1007/s10040-014-1173-6.

Lauber, U., Kotyla, P., Morche, D., Goldscheider, N., 2014. Hydrogeology of an Alpine rockfall aquifer system and its role in flood attenuation and maintaining baseflow. Hydrol. Earth Syst. Sci. 18 (11), 4437. https://doi.org/10.5194/hess-18-4437-2014.

Liu, Z., Tian, L., Yao, T., Yu, W., 2008. Seasonal deuterium excess in Nagqu precipitation: influence of moisture transport and recycling in the middle of Tibetan Plateau. Environ. Geol. 55 (7), 1501–1506. https://doi.org/10.1007/s00254-007-1100-4.

López-Moreno, J.I., García-Ruiz, J.M., 2004. Influence of snow accumulation and snowmelt on streamflow in the central Spanish Pyrenees/Influence de l'accumulation et de la fonte de la neige sur les écoulements dans les Pyrénées centrales espagnoles. Hydrol. Sci. J. 49 (5)https://doi.org/10.1623/hysj.49.5.787.55135.

López-Moreno, J.I., Goyette, S., Beniston, M., 2008. Climate change prediction over complex areas: spatial variability of uncertainties and predictions over the Pyrenees from a set of regional climate models. Int. J. Climatol. 28 (11), 1535–1550. https://doi.org/10.1002/joc.1645.

López-Moreno, J.I., Revuelto, J., Rico, I., Chueca-Cía, J., Julián, A., Serreta, A., Serrano, E., Vicente-Serrano, S.M., Azorin-Molina, C., Alonso-González, E., García-Ruiz, J.M., 2016. Thinning of the Monte Perdido Glacier in the Spanish Pyrenees since 1981. Cryosphere 10 (2), 681–694. https://doi.org/10.5194/tc-10-681-2016.

Mądrala, M., Wąsik, M., Małoszewski, P., 2017. Interpretation of environmental tracer data for conceptual understanding of groundwater flow: an application for fractured aquifer systems in the Kłodzko Basin, Sudetes, Poland. Isot. Environ. Health Stud. 53 (5), 466–483. https://doi.org/10.1080/10256016.2017.1330268.

Malard, A., Jeannin, P.Y., Vouillamoz, J., et al., 2015. An integrated approach for catchment delineation and conduit-network modeling in karst aquifers: application to a site in the Swiss tabular Jura. Hydrogeol. J. 23 (1), 1341–1357. https://doi.org/10.1007/s10040-015-1287-5.

Malard, A., Sinreich, M., Jeannin, P.Y., 2016. A novel approach for estimating karst groundwater recharge in mountainous regions and its application in Switzerland. Hydrol. Process. 30 (13), 2153–2166. https://doi.org/10.1002/hyp.10765.

Malík, P., Svasta, J., Michalko, J., Gregor, M., 2016. Indicative mean transit time estimation from $\delta^{18}O$ values as groundwater vulnerability indicator in karst-fissure aquifers. Environ. Earth Sci. 75, https://doi.org/10.1007/s12665-016-5791-2.

Małoszewski, P., Rauert, W., Stichler, W., Herrmann, A., 1983. Application of flow models in an alpine catchment area using tritium and deuterium data. J. Hydrol. 66, 319–330. https://doi.org/10.1016/0022-1694(83)90193-2.

Maloszewski, P., Rauert, W., Trimborn, P., Herrmann, A., Rau, R., 1992. Isotope hydrological study of mean transit times in an alpine basin (Wimbachtal, Germany). J. Hydrol. 140, 343–360. https://doi.org/10.1016/0022-1694(92)90247-S.

Małoszewski, P., Zuber, A., 1996. Lumped Parameter Models for the Interpretation of Environmental Tracer Data. Manual on Mathematical Models in Isotope Hydrology. IAEA-TECDOC 910. IAEA, Vienna (Austria), 1996.

Małoszewski, P., Zuber, A., 2002. Manual on Lumped Parameter Models Used for the Interpretation of Environmental Tracer Data in Groundwaters (IAEA-UIAGS/CD-02-00131). International Atomic Energy Agency (IAEA) https://inis.iaea.org/search/search.aspx?orig_q=RN:33037906Accessed 4 December 2018.

Marti, R., Gascoin, S., Houet, T., Ribière, O., Laffly, D., Condom, T., Monnier, S., Schmutz, M., Camerlynck, C., Tihay, J.P., Soubeyroux, J.M., 2015. Evolution of Ossoue Glacier (French Pyrenees) since the end of the Little Ice Age. Cryosphere 9 (5), 1773–1795. https://doi.org/10.5194/tc-9-1773-2015.

Martos-Rosillo, S., González-Ramón, A., Jiménez-Gavilán, P., Andreo, B., Durán, J.J., Mancera, E., 2015. Review on groundwater recharge in carbonate aquifers from SW Mediterranean (Betic Cordillera, S Spain). Environ. Earth Sci. 74, 7571. https://doi.org/10.1007/s12665-015-4673-3.

Martos-Rosillo, S., Marín-Lechado, C., Pedrera, A., Vadillo, I., Motyka, J., Molina, J.L., Ortiz, P., Martín-Ramírez, J.M., 2014. Methodology to evaluate the renewal period of carbonate aquifers: a key tool for their management in arid and semiarid regions, with the example of Becerrero aquifer, Spain. Hydrogeol. J. 22 (3), 679–689. https://doi.org/10.1007/s10040-013-1086-9.

Merz, R., Blöschl, G., 2004. Regionalisation of catchment model parameters. J. Hydrol. 287 (1–4), 95–123. https://doi.org/10.1016/j.jhydrol.2003.09.028.

Milano, M., Ruelland, D., Fernandez, S., Dezetter, A., Fabre, J., Servat, E., Fritsch, J.M., Ardoin-Bardin, S., Thivet, G., 2013. Current state of Mediterranean water resources and future trends under climatic and anthropogenic changes. Hydrol. Sci. J. 58 (3), 498–518. https://doi.org/10.1080/02626667.2013.774458.

Molina, A., Melgarejo, J., 2016. Water policy in Spain: seeking a balance between transfers, desalination and wastewater reuse. Int. J. Water Resour. Dev. 32 (5), 781–798. https://doi.org/10.1080/07900627.2015.1077103.

Mook, W.G., De Vries, J.J., 2000. Volume I, Introduction: Theory Methods Review. Environmental Isotopes in the Hydrological Cycle—Principles and Applications, International Hydrological Programme (IHP-V). Technical Documents in Hydrology (IAEA/UNESCO) No, 39. vol. 1, http://www-naweb.iaea.org/napc/ih/IHS_publication.htmlAccessed 4 December 2018.

Mudarra, M., Andreo, B., 2011. Relative importance of the saturated and the unsaturated zones in the hydrogeological functioning of karst aquifers: the case of Alta Cadena (Southern Spain). J. Hydrol. 397, 263–280. https://doi.org/10.1016/j.jhydrol.2010.12.005.

Mudarra, M., Andreo, B., 2015. In: Andreo, B., Carrasco, F., Durán, J.J., Jiménez, P., LaMoreaux (Eds.), Role of the Soil-Epikarst-Unsaturated Zone in the Hydrogeological Functioning of Karst Aquifers. The Case of the Sierra Gorda de Villanueva del Trabuco Aquifer (Southern Spain). Hydrogeological and Environmental Investigations in Karst Systems. Series: Environmental Earth Sciences Springer, (638 pp).

Mudarra, M., Andreo, B., Marín, A.I., Vadillo, I., Barberá, J.A., 2014. Combined use of natural and artificial tracers to determine the hydrogeological functioning of a karst aquifer: the Villanueva del Rosario system (Andalusia, southern Spain). Hydrogeol. J. 22 (5), 1027–1039. https://doi.org/10.1007/s10040-014-1117-1.

Nimon, K.F., Oswald, F.L., 2013. Understanding the results of multiple linear regression: beyond standardized regression coefficients. Organ. Res. Methods 16 (4), 650–674.

Nogués-Bravo, D., Araújo, M.B., Lasanta, T., López-Moreno, J.I., 2008. Climate change in Mediterranean mountains during the 21st century. AMBIO J. Hum. Environ. 37 (4), 280–285. https://doi.org/10.1579/0044-7447(2008)37[280:CCIMMD]2.0.CO;2.

Obleitner, F., 1994. Climatological features of glacier and valley winds at the Hintereisferner (Ötztal Alps, Austria). Theor. Appl. Climatol. 49 (4), 225–239. https://doi.org/10.1007/BF00867462.

Ozyurt, N.N., Bayari, C.S., 2008. Temporal variation of chemical and isotopic signals in major discharges of an alpine karst aquifer in Turkey: implications with respect to response of karst aquifers to recharge. Hydrogeol. J. 16, 297–309. https://doi.org/10.1007/s10040-007-0217-6.

Ozyurt, N.N., Lutz, H.O., Hunjak, T., Mance, D., Roller-Lutz, Z., 2014. Characterization of the Gacka River basin karst aquifer (Croatia): hydrochemistry, stable isotopes and tritium-based mean residence times. Sci. Total Environ. 87, 245–254. https://doi.org/10.1016/j.scitotenv.2014.04.018.

Pardo-Igúzquiza, E., Durán, J.J., Luque-Espinar, J.A., Robledo-Ardila, P.A., Martos-Rosillo, S., Guardiola-Albert, C., Pedrera, A., 2015. Karst massif susceptibility from rock matrix, fracture and conduit porosities: a case study of the Sierra de las Nieves (Málaga, Spain). Environ. Earth Sci. 74, 7583–7592. https://doi.org/10.1007/s12665-015-4545-x.

Peel, M.C., Finlayson, B.L., McMahon, T.A., 2007. Updated world map of the Köppen–Geiger climate classification. Hydrol. Earth Syst. Sci. 11, 1633–1644. https://doi.org/10.5194/hess-11-1633-2007.

Poage, M.A., Chamberlain, C.P., 2001. Empirical relationships between elevation and the stable isotope composition of precipitation and surface waters: considerations for studies of paleoelevation change. Am. J. Sci. 301 (1), 1–15. https://doi.org/10.2475/ajs.301.1.1.

René, P., 2013. Glaciers des Pyrénées: le réchauffement climatique en images, (Éd. Cairn).

Ribalaygua, J., Pino, M.R., Pórtoles, J., Roldán, E., Gaitán, E., Chinarro, D., Torres, L., 2013. Climate change scenarios for temperature and precipitation in Aragón (Spain). Sci. Total Environ. 463, 1015–1030. https://doi.org/10.1016/j.scitotenv.2013.06.089.

Rodgers, P., Soulsby, C., Waldron, S., 2005. Stable isotope tracers as diagnostic tools in upscaling flow path understanding and residence time estimates in a mountainous mesoscale catchment. Hydrol. Process. 19 (11), 2291–2307. https://doi.org/10.1002/hyp.5677.

Ruiz-Constán, A., Marín-Lechado, C., Martos-Rosillo, S., Fernández-Leyva, C., García-Lobón, J.L., Pedrera, A., López-Geta, J.A., Hernández-Bravo, J.A., Rodríguez-Hernández, L., 2015. Methodological procedure for evaluating storage reserves in carbonate aquifers subjected to groundwater mining: The Solana Aquifer (Alicante, SE Spain). In: Hydrogeological and Environmental Investigations in Karst Systems. Springer, Berlin, Heidelberg, pp. 255–262. https://doi.org/10.1007/978-3-642-17435-3_28.

Sánchez-Murillo, R., Brooks, E.S., Elliot, W.J., Boll, J., 2015. Isotope hydrology and baseflow geochemistry in natural and human-altered watersheds in the Inland Pacific Northwest, USA. Isot. Environ. Health Stud. 51 (2), 231–254. https://doi.org/10.1080/10256016.2015.1008468.

Schotterer, U., Froehlich, K., Stichler, W., Trimborn, P., 1993. Temporal variation of ^{18}O and deuterium excess in precipitation, river and spring waters in Alpine re-

gions of Switzerland. In: Isotope Techniques in the study of Past and Current Environmental Changes in the Hydrosphere and the Atmosphere, Edited by IAEA. Proceedings series, ISSN 0074-1884, STI/PUB/908, ISBN 92-0-103293-5 https://inis.iaea.org/search/search.aspx?orig_q=RN:25027909Accessed 4 December 2018.

Seibert, J., 2005. HBV Light Version 2. User's Manual. Uppsala University, Dept. of Earth Science, Hydrology, Uppsala, Sweden.

Seibert, J., Jenicek, M., Huss, M., Ewen, T., 2015. Snow and ice in the hydrosphere. In: Snow and Ice-Related Hazards, Risks and Disasters. pp. 99–137, ISBN: 978-0-12-394849-6 https://doi.org/10.1016/B978-0-12-394849-6.00004-4.

Seibert, J., Vis, M.J.P., 2012. Teaching hydrological modelling with a user-friendly catchment-runoff-model software package. Hydrol. Earth Syst. Sci. 16 (9), 3315–3325. https://doi.org/10.5194/hess-16-3315-2012, 102012.

Solder, J.E., Stolp, B.J., Heilweil, V.M., Susong, D.D., 2016. Characterization of mean transit time at large springs in the Upper Colorado River Basin, USA: a tool for assessing groundwater discharge vulnerability. Hydrogeol. J. 24 (8), 2017–2033. https://doi.org/10.1007/s10040-016-1440-9.

Staudinger, M., Stoelzle, M., Seeger, S., Seibert, J., Weiler, M., Stahl, K., 2017. Catchment water storage variation with elevation. Hydrol. Process. 31 (11), 2000–2015. https://doi.org/10.1002/hyp.11158.

Turk, J., Malard, A., Jeannin, P.-Y., Petric, M., Gabrovšek, F., Ravbar, N., Vouillamoz, J., Slabe, T., Sordet, V., 2015. Hydrogeological characterization of groundwater storage and drainage in an alpine karst aquifer (the Kanin massif, Julian Alps). Hydrol. Process. 29 (8), 1986–1998. https://doi.org/10.1002/hyp.10313.

Turnadge, C., Smerdon, B.D., 2014. A review of methods for modelling environmental tracers in groundwater: advantages of tracer concentration simulation. J. Hydrol. 519, 3674–3689. https://doi.org/10.1016/j.jhydrol.2014.10.056.

Uhlenbrook, S., Seibert, J.A.N., Leibundgut, C., Rodhe, A., 1999. Prediction uncertainty of conceptual rainfall-runoff models caused by problems in identifying model parameters and structure. Hydrol. Sci. J. 44 (5), 779–797. https://doi.org/10.1080/02626669909492273.

Vergés, J., 1999. Estudi geològic del vessant Sud del Pirineu Oriental i central. Evolució Cinemàtica en 3D. PhD Thesis University of Barcelona (UB), Faculty of Geology, 180.

Vicente-Serrano, S.M., Lopez-Moreno, J.I., Beguería, S., Lorenzo-Lacruz, J., Sanchez-Lorenzo, A., García-Ruiz, J.M., Azorin-Molina, C., Morán-Tejeda, E., Revuelto, J., Trigo, R., Coelho, F., Espejo, F., 2014. Evidence of increasing drought severity caused by temperature rise in southern Europe. Environ. Res. Lett. 9 (4), 044001. https://doi.org/10.1088/1748-9326/9/4/044001.

Vitvar, T., Gurtz, O., Lang, H., 1999. Application of GIS-based distributed hydrological modelling for estimation of water residence times in the small Swiss pre-alpine catchment Rietholzbach. Integrated Methods in Catchment Hydrology—Tracer. In: Remote Sensing and New Hydrometric Techniques (Proceedings of IUGG 99 Symposium HS4, Birmingham, July 1999). IAHS Publ. no. 258, 1999

Viville, D., Ladouche, B., Bariac, T., 2006. Isotope hydrological study of mean transit time in the granitic Strengbach catchment (Vosges Massif, France). Application of the FlowPC model with modified input function. Hydrol. Process. 20, 1737–1751. https://doi.org/10.1002/hyp.5950.

Viviroli, D., Dürr, H.H., Messerli, B., Meybeck, M., Weingartner, R., 2007. Mountains of the world—water towers for humanity: typology, mapping and global significance. Water Resour. Res. 43 (7), W07447. https://doi.org/10.1029/2006WR005653.

Viviroli, D., Weingartner, R., 2004. The hydrological significance of mountains: from regional to global scale. Hydrol. Earth Syst. Sci. 8, 1016–1029. https://doi.org/10.5194/hess-8-1017-2004.

Wassenaar, L.I., Ahmad, M., Aggarwal, P., van Duren, M., Pöltenstein, L., Araguas, L., Kurttas, T., 2012. Worldwide proficiency test for routine analysis of δ2H and $\delta^{18}O$ in water by isotope-ratio mass spectrometry and laser absorption spectroscopy. Rapid Commun. Mass Spectrom. 26 (15), 1641–1648. https://doi.org/10.1002/rcm.6270.

Wetzel, K., 2004. On the hydrogeology of the Partnach area in the Wetterstein Mountains (Bavarian Alps). Erdkunde 58, 172–186 http://www.jstor.org/stable/25647659.

Zini, L., Casagrande, G., Calligaris, C., Cucchi, F., Manca, P., Treu, F., Zavagno, E., Biolchi, S., 2015. In: Andreo, B., Carrasco, F., Durán, J.J., Jiménez, P., LaMoreaux (Eds.), The Karst Hydrostructure of the Mount Canin (Julian Alps, Italy and Slovenia). Hydrogeological and Environmental Investigations in Karst Systems. Series: Environmental Earth Sciences Springer, p. 638. https://doi.org/10.1007/978-3-642-17435-3.